Standard Model Higgs Detection and Measurements at a Linear Collider

GEORGIOS CHOUDALAKIS

ABSTRACT

The Higgs boson is believed to be one of the fundamental constituents of the Standard Model. In this work I am firstly presenting the significance of the Higgs Mechanism and what has been achieved so far in the experimental search for it. Then, I will investigate how a Linear Collider should be to designed to improve our knowledge of its properties. Finally I am going to present an outline of the method that would allow a compelling measurement of its properties, focussing on the measurement of its mass.

Contents

1 Motivation

In accelerator experiments physicists probe the way elementary particles interact. Excluding experiments with cosmic radiation (CR), we have investigated how nature works at collisions of energy up to 1.96 TeV. This is the center-of-momentum energy at Tevatron, currently the most powerful accelerator. LHC is expected to operate by 2008, stretching this frontier to 14 TeV.

The Standard Model (SM) has been extremely successful at describing almost all phenomena we have observed so far in this energy range [1, 2, 3]. However, we still ignore *the mechanism* that causes some of the phenomena we see, first being the fact that $W^{\pm}$, Z, quarks and leptons (including neutrinos [4]) are massive particles.

For the particles to be given masses, it is necessary to break in some way the symmetry of the electroweak interaction. If the SM were just a mathematical conception instead of a model intending to describe the real world, the demand for local gauge invariance of electroweak interaction would be satisfied even without any mass terms in the Lagrangian [5]. But masses must somehow be introduced in the Model. One may think that it would be a good idea to manually plug mass terms in the Lagrangian of the SM, but it can be proved that this naive method would make the theory unrenormalizable.

The Higgs scalar field is only one mechanism of electroweak symmetry breaking; other approaches, based on very different dynamics, also exist. For example, one can introduce new fermions and new dynamics (*i.e.*, new forces[8, 9]), or implement Higgs in the context of Supersymmetry (SUSY)[10]. Though there is no direct observation of the Higgs Boson, there are indications that can be interpreted as favoring its existence, as we will see in the next section.

The significance of the question of the existence of Higgs is obvious. If it exists, as the majority of physicists expects today, then its discovery would advance our confidence and trust in the SM to an even higher level. Then, the SM would become a *renormalizable* theory which succeeds to explain the fact that particles have mass. The involvement of Higgs in important phenomena, such as CP violation and renormalizability, makes the determination of its properties a requirement to understand better the behaviour of quarks and leptons. Its observation, and the check whether it is a SM Higgs or one of the particles that SUSY predicts for example is important because if SUSY is a correct theory then Particle Physics goals will turn to the direction of determining the parameters of SUSY and checking if this SM extension can answer issues that are not yet understood, such as the apparent plentiness of dark matter, the hierarchy puzzle, the nature of gravity, Grand Unification etc.

Also, the mass of the Higgs is correlated with the scale of energy Λ at which the SM is expected to fail describing things right. We know that at some energy lower than the Planck energy $M_{PL} \simeq 10^{19} GeV$, this failure has to happen, since gravity is not included in the SM (fig. 1). Even more funtamentally and within the energies we have already studied, the SM needs the Higgs boson to exist so as the cross-sections of several SM processes (such as $u\bar{u} \to W^+W^-$) not to diverge.
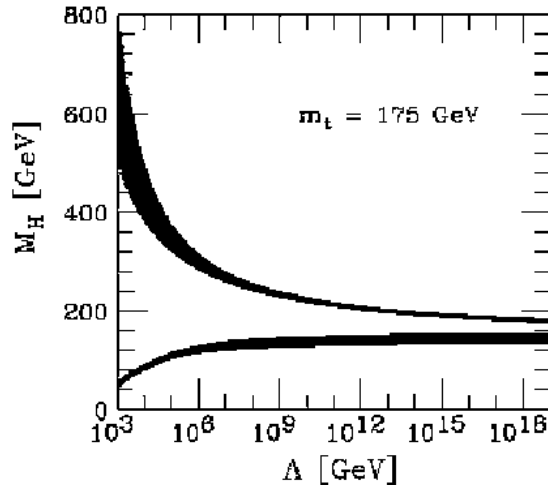
Figure 1: The dependence of the Higgs mass M_H and the energy scale Λ at which the SM is expected to break down. If $M_H \approx 120 GeV$, then the SM appears to extend up to the Planck scale. Actually, Supersymmetry is expected to take over much before M_{PL}, even if M_H is in that small window.

On the other hand, if Higgs is not observed, then alternative theories will need to be investigated more carefully, possibly giving raise to new experiments. New theories might be motivated, or theories like Strings Theory may gain ground, proposing alternative approaches to the puzzles of particles.

Before even being observed, Higgs has inspired hundreds of thousands of publications, involving almost all areas of Particle Physics, from renormalizability [12] to extra-dimensions theories and Superstrings[13]. This is a characteristic indication of its great importance which justifies its popularity.

1.1   Outline of the Higgs Mechanism

The Higgs Mechanism is one possible answer to the puzzle of mass acquisition. The rigorous description of the Mechanism has been done by several authors ([7, 5, 6]), so here we are going to describe only its outline with two examples.

In essence, the assumption is made that the universe is filled with a spin-zero field, called a Higgs field, that is a doublet in the $SU(2)$ space and carries non-zero $U(1)$ hypercharge and also is a color singlet. In the presence of this field gauge bosons and fermions appear to have non-zero mass.

The simplest example of spontaneous symmetry breaking is to consider a Lagrangian

$$\mathcal{L} = T - V = \frac{1}{2}\partial_\mu\phi\partial^\mu\phi - \left(\frac{1}{2}\mu^2\phi^2 + \frac{1}{4}\lambda\phi^4\right). \tag{1}$$

This potential V is symmetric under $\phi \to -\phi$. For $\lambda > 0$, if $\mu^2 = 0$ then the vacuum, which

4

is the ϕ that minimizes V, corresponds to $\phi = 0$. But there is no physical reason for μ^2 to be positive. If $\mu^2 < 0$ then the potential V has two minima, corresponding to

$$\phi = \pm\sqrt{\frac{-\mu^2}{\lambda}} \equiv v. \tag{2}$$

So, the (Higgs) field has a non-zero value in the vacuum.

To determine the particle spectrum, we must study the theory in the region of the minimum, so we put

$$\phi(x) = v + \eta(x) \tag{3}$$

so that we are expanding around $\eta = 0$. We could have chosen to expand around the negative minimum $(-v)$, which would give the same physics. This arbitrariness is the reason we talk about spontaneous symmetry breaking. After substitution of (3) in the $\mathcal{L}$, we get an expression for the Lagrangian which is

$$\mathcal{L} = \frac{1}{2}(\partial_\mu \eta \partial^\mu \eta) - \left(\lambda v^2 \eta^2 + \lambda v \eta^3 + \frac{1}{4}\lambda \eta^4\right) + \text{constant}. \tag{4}$$

Now, instead of a $\mathcal{L}$ of the field ϕ we have a $\mathcal{L}$ of the perturbation η. This Lagrangian represents the description of a (Higgs) particle with mass

$$m_\eta^2 = 2\lambda v^2 = -2\mu^2, \tag{5}$$

deriving from its self-interaction.

Similarly we need to work on a $U(1)$ or $SU(2)$ symmetric Lagrangian to attribute mass to the corresponding vector bosons, Z^0 and $W^\pm$.

For the $U(1)$ case, we can start from a complex scalar field $\phi = (\phi_1 + i\phi_2)/\sqrt{2}$, and

$$\mathcal{L} = (\partial_\mu \phi)^*(\partial^\mu \phi) - \mu^2 \phi^* \phi - \lambda(\phi^* \phi)^2. \tag{6}$$

As before, $\mu^2 < 0$. To make $\mathcal{L}$ invariant under *local* $U(1)$ gauge transformations $\phi(x) \rightarrow \phi'(x) = e^{i\chi(x)}\phi(x)$, we must rewrite it in terms of the covariant derivative $\mathcal{D}_\mu = \partial_\mu - igA_\mu$, simultaneously introducing the gauge field, transforming as $A_\mu \rightarrow A'_\mu = A_\mu - \frac{1}{g}\partial_\mu \chi(x)$. The Lagrangian is then

$$\mathcal{L} = (\mathcal{D}_\mu \phi)^*(\mathcal{D}^\mu \phi) - \mu^2 \phi^* \phi - \lambda(\phi^* \phi)^2 - \frac{1}{4}F_{\mu\nu}F^{\mu\nu}. \tag{7}$$

The potential energy has a minimum along circle of radius $\phi_1^2 + \phi_2^2 = -\frac{\mu^2}{\lambda} = v^2$. The typical perturbation method is now to expand ϕ around a point along this circle:

$$\phi = \frac{(v + \eta(x) + i\rho(x))}{\sqrt{2}} \tag{8}$$

Because of the local gauge invariance, we have the freedom to rewrite the field in the form $\phi(x) = \frac{(v+h(x))}{\sqrt{2}}$. Then,

$$\mathcal{L} = \frac{1}{2}(\partial_\mu h)(\partial^\mu h) + \frac{1}{2}g^2 v^2 A_\mu A^\mu - \lambda v^2 h^2 - \lambda v h^3$$
$$-\frac{\lambda}{4}h^4 + g^2 v h A^\mu A_\mu + \frac{1}{2}g^2 h^2 A_\mu A^\mu - \frac{1}{4}F_{\mu\nu}F^{\mu\nu}. \tag{9}$$

Remarkably, we see that the gauge boson A has mass $M_A = gv$. If we had substituted ϕ as it is parametrized in eq. (8), we would have ended up with one massless boson term in the Lagrangian. This is the renouned Goldstone boson. Using this alternative parametrization, this unnatural boson has given its place to a third (longitudinal) polarization that the massive A_μ can have.

The process to apply the Higgs Mechanism for an $SU(2)$ local gauge invariant field is analogous, just more mathematically tedious.

2 History

As a result of the very high interest in the Higgs boson, a lot of intense research has already been conducted in the direction of

- directly detecting the Higgs, and

- constraining its mass from electroweak precision measurements

The most important experiments that have contributed to this research are those that ran at LEP (Large Electron Positron collider), SLC (Stanford Linear Collider) and Tevatron, located at CERN, SLAC and Fermilab respectively. Efforts for *direct* observation of the Higgs at those experiments has been fruitless [11, 50]. What has been achieved however is the combination of several other SM measurements, which are sensitive to the mass of the Higgs, in order to *indirectly* set constrains for its mass.

2.1 How the SM gives hints about m_H

Physicists have been trying to put constrains to m_H by measuring very precisely other parameters of the SM which are related to m_H. The first thing that should be pointed out is that whenever such an attempt is made, one has to *assume* the correctness of some model, and based on that assumption he can proceed. As mentioned, the MSM (Minimal Standard Model) can not be a complete theory, since it is expected to break down at some energy scale Λ. But the mass of the Higgs is expected to be lower than 1 TeV, so probably the assumption of a MSM is numerically accurate enough.

A SM Higgs would affect all currently measured electroweak observables, primarily through correction in the polarization of vacuum to W and Z bosons, through diagrams like those in fig. 2.
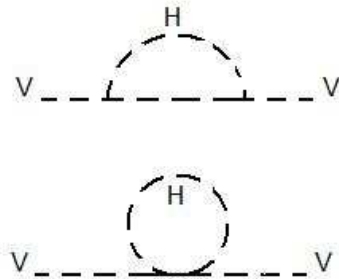

Figure 2: Vacuum polarization to W and Z vector bosons, denoted by V.

More specifically, the parameters that are mostly used to constrain the MSM Higgs mass are m_W and $sin^2\theta_w$. Those parameters are related to the m_H by the following two expressions [15]:
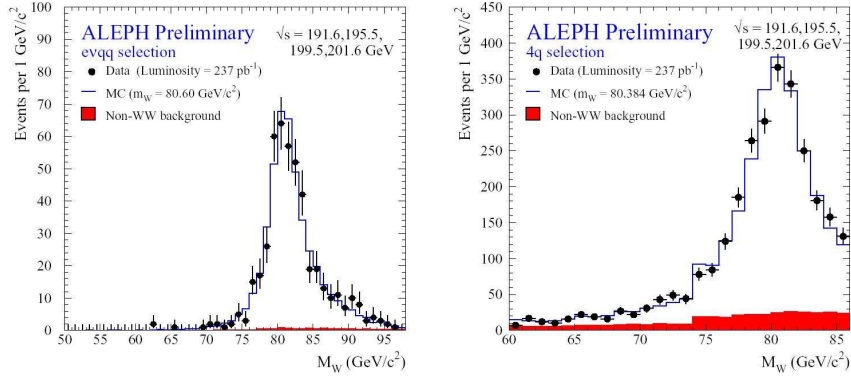
Figure 3: Invariant mass distribution of two different final states of W decays at ALEPH.

$$m_W = \quad 80.3805 - 0.0581 \ln \frac{m_H}{100 \text{ GeV}} - 0.0078 \ln^2 \frac{m_H}{100 \text{ GeV}}$$
$$-0.518 \left[\frac{\Delta\alpha_{had}^5}{0.0280} - 1 \right] + 0.537 \left[\left(\frac{m_t}{175 \text{ GeV}} \right)^2 - 1 \right]$$
$$-0.085 \left[\frac{\alpha_s(M_Z)}{0.118} - 1 \right] \tag{10}$$

$$\sin^2 \theta_W^{eff} = \quad 0.231540 + 5.23 \cdot 10^{-4} \ln \frac{m_H}{100 \text{ GeV}}$$
$$+0.00986 \left[\frac{\Delta\alpha_{had}^5}{0.0280} - 1 \right] - 0.00268 \left[\left(\frac{m_t}{175 \text{ GeV}} \right)^2 - 1 \right]$$
$$+4.4 \cdot 10^{-4} \left[\frac{\alpha_s(M_Z)}{0.118} - 1 \right] \tag{11}$$

From equations 10 and 11 it is obvious that, except for m_W and $\sin \theta_W^{eff}$, we also need to know the parameters $\Delta\alpha_{had}^5$, m_t and $\alpha_s(M_Z)$. Another remark is that m_H is met as an argument of the log function, which means that its errors are multiplicative, instead of additive.

2.1.1 Knowledge of the m_W

The mass of the W boson has been measured at experiments at Tevatron (CDF, D0) [16] and at CERN (LEP II) [17]. Precise determination has been achieved using $W \to q\bar{q}q\bar{q}$ and $q\bar{q}\ell\bar{\nu}_\ell$ processes (fig. 3).

The world average of the m_W presently is 80.426 ± 0.034 [18], but there are several different assumptions which can be made, resulting into slightly different estimations. An overview of the experimental results for the W mass is in fig. 4.
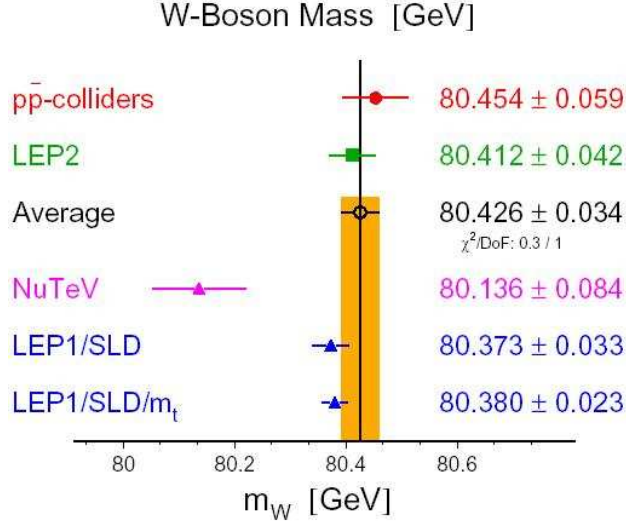
Figure 4: Different measurements of the W mass.

2.1.2 Knowledge of the $\sin\theta_W^{eff}$

The effective weak mixing angle for the $Z - \ell^+\ell^-$ coupling is defined in terms of the vector and axial vector effective couplings,

$$\sin^2\theta_W^{eff} = (1 - v_\ell/\alpha_\ell)/4, \tag{12}$$

and is also related to the left-right coupling asymmetry [19]:

$$A_\ell = \frac{(g_L^\ell)^2 - (g_R^\ell)^2}{(g_L^\ell)^2 + (g_R^\ell)^2} = \frac{2v_\ell\alpha_\ell}{v_\ell^2 + \alpha_\ell^2} = \frac{2(1 - 4\sin^2\theta_W^{eff})}{1 + (1 - 4\sin^2\theta_W^{eff})^2} \tag{13}$$

The measurement of $\sin^2\theta_W^{eff}$ has mostly been done at SLD and LEP, with analyses which use severel asymmetries where the value of $\sin^2\theta_W^{eff}$ is involved. The world average today is $0.23149(15)$ [20] (fig. 5).

2.1.3 The parameters $\Delta\alpha_{had}^5$, m_t and $\alpha_s(M_Z)$

The top quark mass measurement is still ongoing at experiments mostly at Tevatron [21] where t was first observed. The current value for m_t is $174.3 \pm 5.1\,GeV$ from direct observation and $178.1_{-8.3}^{+10.4}\,GeV$ from SM electroweak fit [22].

The strong coupling constant $\alpha(M_Z)$ is currently measured to be $0.1187(20)$ [20].

The $\Delta\alpha_{had}(M_Z^2)$, defined as

$$\Delta\alpha_{had} = \frac{\alpha(q^2) - \alpha_0}{\alpha(q^2)} = \Pi'_{\gamma\gamma}(q^2) - \Pi'_{\gamma\gamma}(0) \tag{14}$$

9
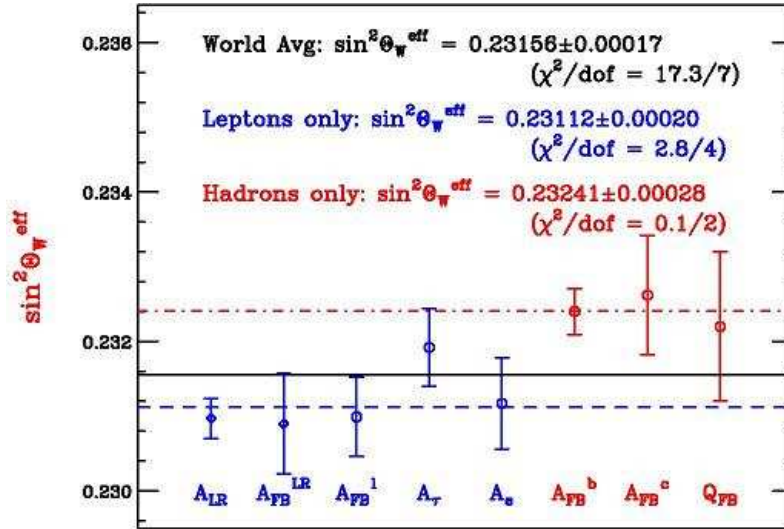
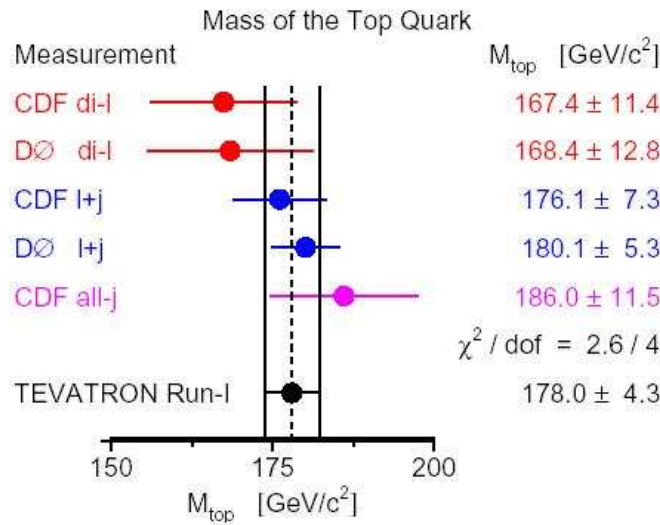Figure 5: Summary of the measurements of $\sin \theta_W^{eff}$ at SLD and LEP by the year 2001.

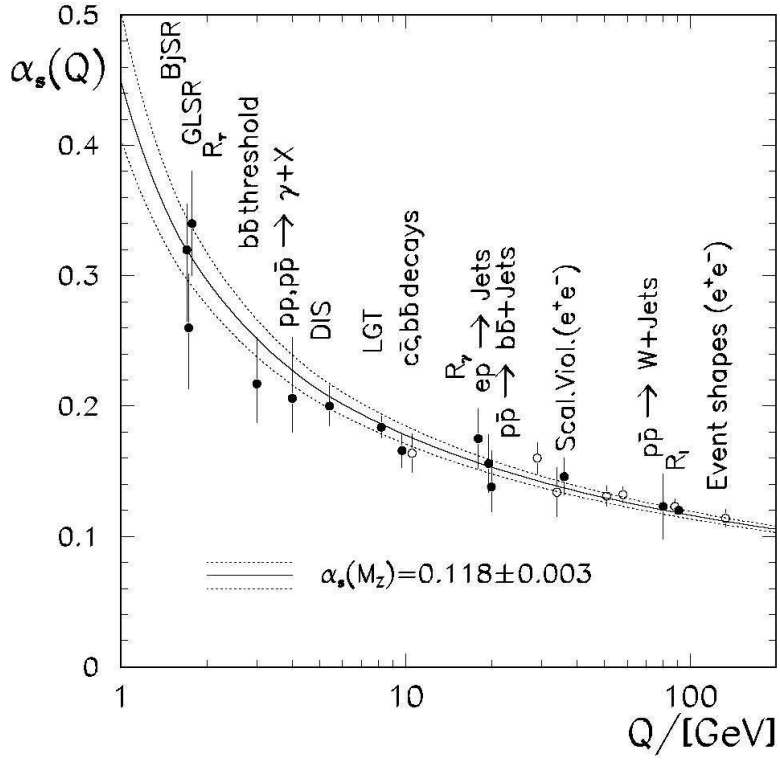Figure 6: Summary of the measurements of m_t at Tevatron.

Figure 7: α_s as a function of energy. Source: [23]

11

Authors	Year	$\Delta\alpha_{had}^{5}(M_Z^2) \ (10^{-4})$
Lynn, et al.	1987	??
Burkhardt et al.	1987	288 ± 9
Jegerlehner	1991	282 ± 9
Martin and Zeppenfeld	1994	273.2 ± 4.2
Swartz	1994/5	275.2 ± 4.5
Eidelman and Jegerlehner	1995	280 ± 7
Burkhardt and Pietrzyk	1995	280 ± 7
Alemany, Davier, and Hocker	1997/8	281.7 ± 6.2
Kuhn and Steinhauser	1998	277.5 ± 1.7
Davier and Hocker	1998	277.1 ± 1.6
Erler	1998/9	277.9 ± 2.0
Martin, Outhwaite, and Ryskin	2000	274.2 ± 2.5
Pietrzyk	2000	275.5 ± 4.6
Burkhardt and Pietrzyk	2001	276.1 ± 3.6

Figure 8: Some of the values calculated for $\Delta\alpha_{had}(M_Z^2)$ by 2001. Red results are mostly data-driven, and blue results are mostly theory driven.

where $\alpha_0 = 1/137.03599911(46)$ [20]. The determination of $\Delta\alpha_{had}(M_Z^2)$ can be done both theoretically and experimentally. Some of its estimated values and errors are summarized in fig. 8.

2.2 Constraints on m_H

From the above discussion it is clear that if we assume the MSM is correct and select some values for the parameters relating to the m_H, we can make a χ^2 test of the m_H against the data. Such a test would indicate which value of m_H is favored under those specific assumptions for the parameters, based on the current measurements. In fig. 9 we see the result of this test [24].

The global fit yields $m_H = 91^{+58}_{-37}$ GeV. This corresponds to a one-sided upper limit at 95% C.L. on m_H of 211 GeV. The shaded part of the plot if fig. 9 corresponds to the area of $m_H < 114.4$ GeV. This area has been excluded at 95% C.L. by experiments searching for direct observation of the Higgs. The minimum of χ^2 lies in the excluded region, but the uncertainties on m_H are such that the MSM Higgs scenario can not be excluded. Also, we should keep in mind that this fit is very sensitive to some of the parameters it uses, such as m_t and $\Delta\alpha_{had}^5$. For example, if the measurement of m_t changes by one standard deviation (which means 5 GeV) then we get a shift of 35% in the predicted m_H.
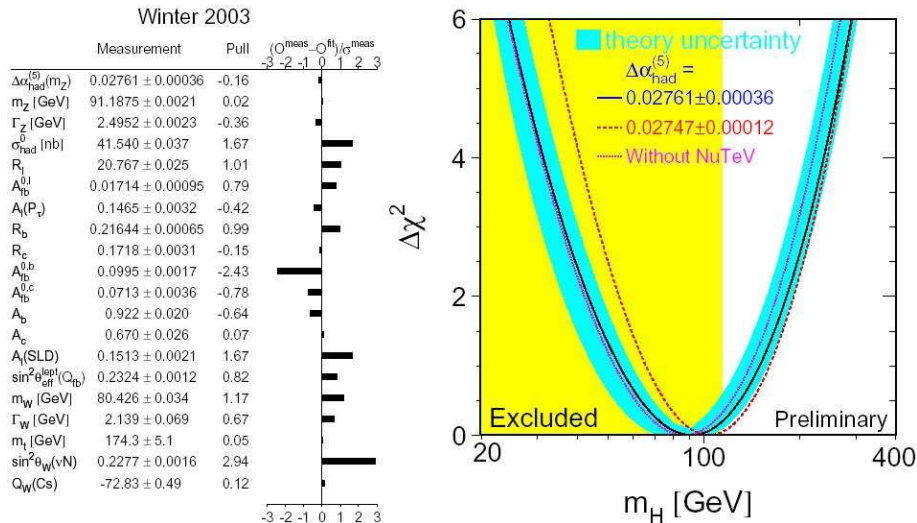
Figure 9: Left: Used data in the electroweak fit and their agreement with the Standard Model; right: $\Delta\chi^2$ as a function of m_H.

3 The Linear Collider

Today the highest energy at which we have ever collided particles has been achieved at Tevatron and is 1.96 TeV $p - \bar{p}$ collisions. This frontier is expected to be extended before the end of this decade to 14 TeV $p - p$ collisions at LHC. Both of those colliders are ring colliders, using magnets to bend and to focuss the proton beams and RF waves to accelerate the particles.

The great advantage of ring colliders is that they allow us to accelerate particles to very high energies by letting them go around the ring as many times as they need to acquire those energies. But there is a price one has to pay. Since particles are accelerated to stay in their circular path, they emmit EM radiation (bremsstrahlung), loosing part of their energy. The lighter the particles, the faster they need to travel to achieve the same energy, and the faster they travel along the ring, the more they radiate. The formula that gives the per turn energy loss for a particle of energy E, mass m and charge e is

$$\Delta E / 2\pi R = 4\pi e^2 \beta^2 \gamma^4 / 3R, \tag{15}$$

where R is the radius of curvature. As a result, it is extremelly inefficient to use light particles, such as electrons, to reach energies higher than a few hundred GeV, like at LEP II.

Instead, hadrons such as protons are used to reach higher energies. But again, there is a price to be paid. Since protons are composite particles interacting mostly hadronically, but QCD is not yet completely understood[1]. Also, the energy distribution and other, more

---

[1] At least, at high energies the strong coupling becomes smaller than unit, allowing us to make perturbative QCD calculations.

or less well known parameters of the structure of the proton have to be taken into account to make reliable theoretical predictions of the outcome of proton collisions. Finally, because of the strong interactions that are allowed, hadronic collisions are much more rich in background than leptonic collisions (e.g. e^+e^-), making it more difficult to separate the signal in several cases. For example, LEP I and LEP II experiments gave us extremelly beautiful and 'clean' results, such as the direct observation of the Z and W bosons. The success of those experiments was partly due to the fact that they collided electrons against positrons (not hadrons).

It would be extremely tempting to repeat e^+e^- collisions at higher energies than those reached at LEP I and II. As soon as LEP reached the energy of 80 GeV, W boson was detected. It is justified to expect that at higher energies new particles, including the SM Higgs, will emerge out of a relatively low background. As explained, ring accelerators would not be able to contribute in this purpose. What is needed is to construct a Linear Collider (LC) which would accelerate electrons and positrons to energies high enough to discover new physics.

The basic features that make a 500 GeV LC an appropriate instrument for research for new physics are summarized here:

- The signal to background ratio in e^+e^- collisions is much higher than in hadronic collisions. The cross sections of several e^+e^- processes can be seen and compared in fig. 10.

- We mostly have to deal with 2-body kinematics, from an initial state with well-defined quantum numbers.

- The processes in e^+e^- collisions are electroweak and thus we know how to calculate them very accurately.

- The electron (and positron) beam may be polarized, allowing selective suppression of backgrounds.

- The collider energy may be varied to optimize the study of particular reactions.

LC technological considerations

Some proposals for Linear Colliders have already been written. TESLA is one of those proposed experiments, intending to perform e^+e^- collisions at 500 and 800 GeV. We will borrow basic ideas and information from proposals such as TESLA to envision a LC free of budget limitations.
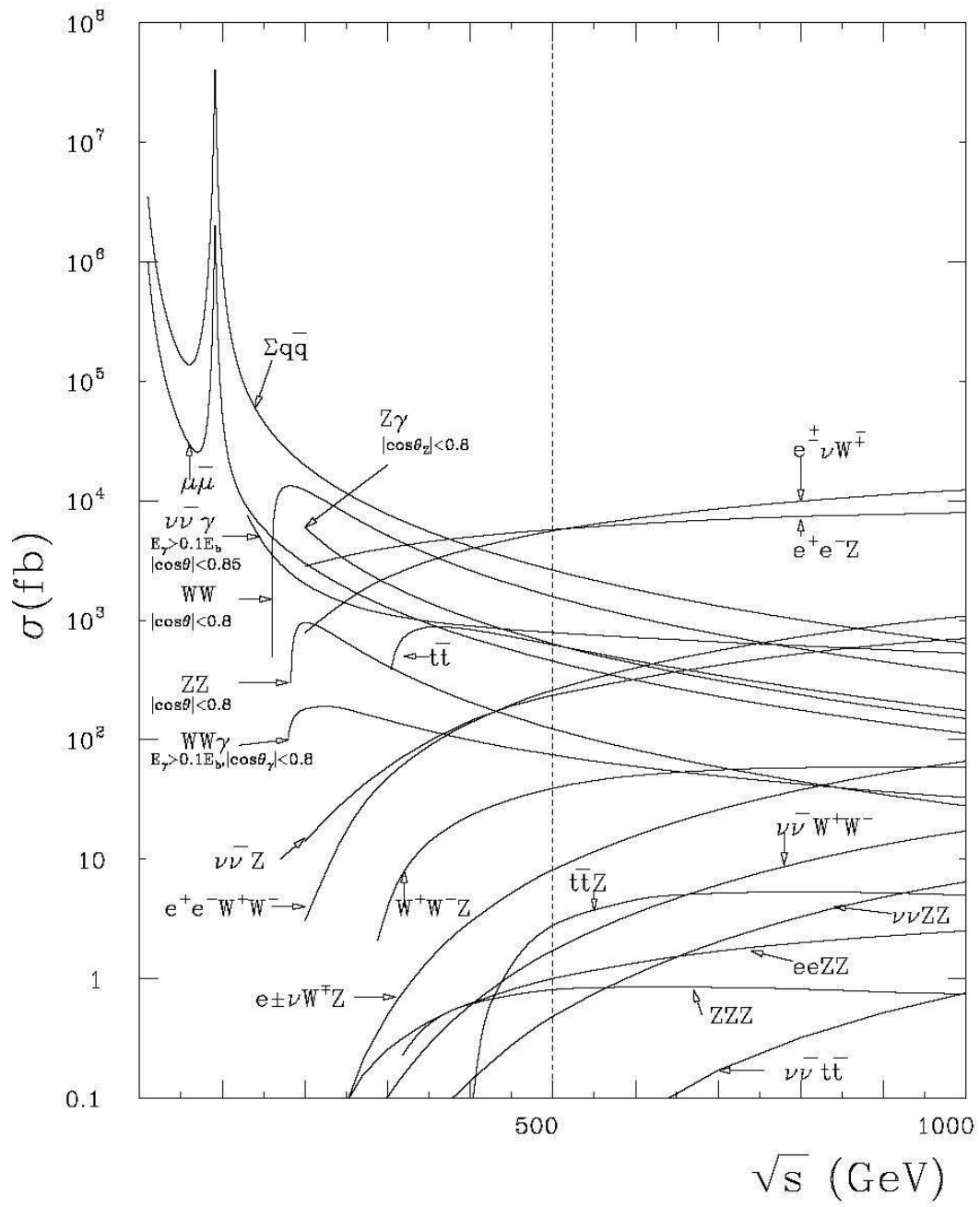
Figure 10: Cross sections for a variety of processes at an e^+e^- LC [30].

15

3.1   The e^+e^- source

First we will describe a way to provide electrons and positrons to the linear accelerators (or lineacs in short).

To produce (unpolarized) electrons is almost trivial, since they are steady particles and plenty of them can be found in ordinary matter. An easy way is to heat up a piece of metal and have them emmited by thermal emission. Alternatively, more efficiently, one can knock electrons out of a semiconductor using by litting it with a laser, like in SLAC. Then, one can set up a positively charged plate nearby, to attract them over, and cut a small hole in it; the electrons that make it through the hole constitute the a beam, which can then be passed through focussing and bending magnets and accelerating devices to acquire the wished properties [29].

A way to get positrons is to produce photons of high enough energy (quiet greater than $2m_e$) and to send them on a thin rotating target, where they convert into e^+e^- pairs. The needed photons can be produced using an electron beam of 150-250 MeV, sent through a long planar undulator magnet placed upstream of the interaction point.

Undulator magnet is a device producing a magnetic field of alternating polarity. When eletrons pass through it they are forced to "wiggle", emitting photons by bremsstrahlung. It is also known as a wiggler magnet.

The produced positrons are emitted in several directions and a system of magnets is needed to collect them and focuss them into a beam.

Something that would help at the search for the Higgs boson would be to have polarized electrons and maybe also polarized positrons. We have much more experience in polarizing electrons than positrons. The production of a polarized electron beam can be done by photoemission from a GaAs photocathode. This is how polarized e^- beam is currently being produced at SLC. A circularly polarized laser beam hits a strained GaAs semiconductor, causing photoexcitation of electrons, which are emitted with the same helicity as the incident photons. In this way we can get a $\sim 80\%$ polarized e^- beam. More details can be found in [31].

To produce a polarized positron beam more sophisticated techniques are required. It has not been done yet, but there is an experiment which has been approved to run in January 2005 at SLAC with the name E-166. At E-166 a polarized positrons beam is going to be produced in the following way [32]: A helical undulator magnet[2] is going to make electrons emit circularly polarized photons of several MeV. Then, they are going to be converted into e^+e^- in a thin (~ 0.5 radiation length) target of Titanium. The polarization of the photons will be transfered to the e^+e^- pair, resulting in longitudinally polarized positrons. Positrons with energy closer to the energy of the incoming photons have higher polarization (close to 100%), while the lower energy positrons are less polarized. That is partly why the Titanium target has to be thin, because otherwise positrons would loose part of their energy (and

---

[2]In a helical undulator the B field is not alternating but helical, i.e. the particle experiences a circularly rotating $\vec{B}$ as it passes through the undulator.

polarization) by bremsstrahlung in the target. The E-166 technique could be used in a LC, and this is part of the motivation of E-166. With proper upgrades we can then produce polarized positron currents, high enough to achieve high luminosity.

The e^- and e^+ beams can not imediately enter the linacs. The reason is that they initially have very high *emittance*. Emittance is a property related to size and density of the particle beam. If the emittance is too big the beam won't fit in its allotted space and that part of the beam is lost. In other words, the lower the emittance, the more parallel the velocities of the particles, the more focussed the beam.

What we need to reduce the emittances of the beams is *damping rings*. Emittance reduction is achieved via the process of radiation damping, i.e. the combination of synchrotron radiation in bending fields with energy gain in RF cavities. So far, the lowest emittance beam has been produced in the Accelerator Test Facility at KEK, in Japan [33]. The operation principle of damping rings is to use dipole and quadrupole magnets, as well as wigglers to collimate the electrons of the beam. Dipoles turn horizontally and vertically the beam to center it, quadrupoles focuss it and wigglers make the energy distribution more uniform, since more energetic particles bremsstrahlung more than less energetic ones. To monitor the dumping ring and fine tune its operation it is very important to have many and high performance BPMs[3].

At KEK we have gained the experience of how to damp electron beams to very low emittance, so if we remove any funding limitations it will be possible to construct very long damping rings, equipped with a large number of magnets and BPMs, producing a well collimated beam for the LC.

3.2 The accelerator

The technique used to accelerate charged particles to high energies is to pass them through RF resonant cavities. At a machine like TESLA, e^+e^- are expected to enter the linear accelerators at the starting energy of 5 GeV, after having been refined in the dumping rings.

The principle of operation of RF acceleration is that every bunch of particles travels along a pipe accompanied by the maximum of the $\vec{E}$ of an electromagnetic wave. In this way it is accelerated all along its passing. The basic components of an RF system include the klystron, the microwave guide and the RF cavities. The klystron generates pulsed RF power from (pulsed) high voltage power, which is then distributed to the cavities by a system of waveguides. (fig. 11).

The most basic characteristic values of an RF system are the accelerating field E_{acc} and the intrinsic quality factor Q_0, which is a number dependent on geometric characteristics and inversely proportional to the surface resistance of the resonant cavity. Q_0 is important to be as high as possible, because low Q_0 not only limits the cavity maximum E_{acc} due to thermal breakdown, but also increases the cost of the cryogenics that keep the temperature

---

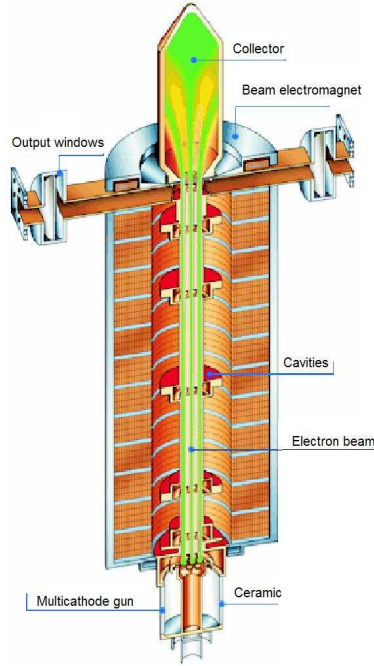[3]Beam Position Monitors, described later.

Figure 11: Sketch of the TH1801 klystron [25].

low [26]. We will consider 9-cell superconducting niobium RF cavities, cooled by superfluid He, whose properties have been studied [27] and which have been improved in many terms (e.g. $1400°C$ heat treatment, electropolishing etc) to achieve high performance.

Studies have shown that cryogenic RF cavities would achieve high enough E_{acc} to reach the energy of 500 GeV without having to make the linear accelerator too long[4] [27]. We will consider an electron and a positron accelerator of length 14.4 Km each, accelerating beams to 250 GeV each, using $10,296$ 9-cell superconductive cavities each. The E_{acc} of those cavities is selected to be 23.4 MV/m, a value at which the Q_0 is still high (see fig. 12).

Along the linacs there also are cryomodules to keep the temperature low (2K) for the cavities to be superconductive, and there also are beam position monitors (BPM), which are used to correct the trajectory of the beam. The corrections are made with bending and quadrupole magnets along the linacs. The bending magnets need to be horizontal and vertical, to correct deflections of the beam in both directions. They are superconductive and they are cooled down by the same cryomodules that cool the cavities. The operation principle of the (pill-box type) BPM (fig. 13) is that it detects the first dipole normal mode TM_{110}, which is excited when a beam crosses it off-centered. The larger the offset of the beam, the stronger the excitation.

That was the very brief description of the linacs, based on the TESLA TDR, which

---

[4]Making it too long would have, of course, financial consequences, but we are not focussing on them here. The problem would mostly be the difficulty of construction and of dealing with the maintenance of the collision point, which is can be lost by the slight vibrations of the structure.
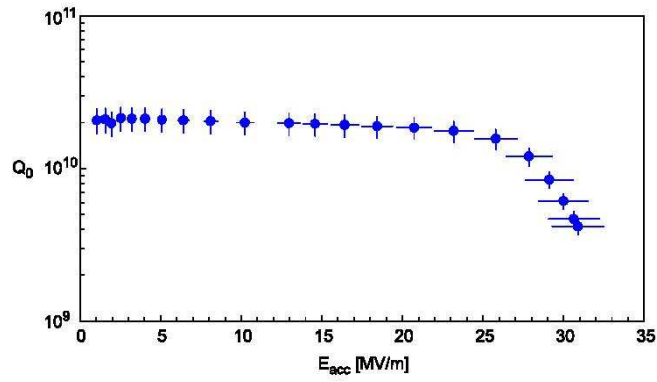
Figure 12: Excitation curve of a high-performance 9-cell cavity. The cavity was cooled by superfluid helium of 2 K. The systematic rms errors in the determination of the accelerating field and the quality factor are indicated [27].
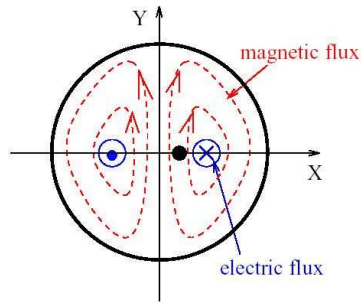

Figure 13: Cross section of the pillbox type BPM [28].

would accelerate electrons and positrons to the energy of 500 GeV. The design for TESLA includes a 800 GeV operation mode, by increasing the E_{acc} of the cavities. So, in principle it is possible to reach higher energies, even up to 1 TeV by upgrading the linacs already described. Especially if we disregard any budget limitations, we can envision a LC longer and stronger that would be able to reach 1 TeV center of mass energy. There are more details about the electronics, the systems that control and synchronize the several parts etc, but this is probably beyond the scope of this work to get into more details.

3.2.1 Luminosity

LHC is going to achieve luminosity of about $10^{34} \, cm^{-2} s^{-1}$ [34]. In order to have useful data in a reasonable amount of operation time, it is believed that we need a $e^+ e^-$ collider with luminosity of at least $10^{33} \, cm^{-2} s^{-1}$ [27]. This number is not greater than the luminosity expected at LHC, however the $e^+ e^-$ collisions provide much lower background events for most processes, so we need less statistics to distinguish the signal from the background.

The key to obtain such high luminosity is the low emittance of the beam, its high population, as well as the small interaction point (IP). There is a formula [27] which connects the luminosity L with beam parameters:

$$L = \frac{n_b N_e^2 f_{rep}}{4\pi \sigma_x^* \sigma_y^*} \times H_D \tag{16}$$

where

$$
\begin{array}{ll}
n_b & \text{number of bunches per pulse} \\
N_e & \text{number of electrons (or positrons) per bunch} \\
f_{rep} & \text{pulse repetition frequency} \\
\sigma_{x,y}^* & \text{horizontal (or vertical) beam size at the IP} \\
\sigma_z & \text{bunch length at IP} \\
H_D & \text{disruption enhancement factor (typically } H_D \approx 2)
\end{array}
$$

From 16 it seems that if we make the beam extremely thin we will have extremely high L. This is true, however there is a side effect which is affected by the cross section of the beam; when the electrons and the positrons approach each other they experience mutual attraction, which accelerates them and they produce forward electromagnetic radiation. This kind of "linear" bremsstrahlung, which is also called *beamstrahlung*, is extremely less significant than the bremsstrahlung we have in accelerating rings, but must be taken into consideration, because it can produce extra $e^+ e^-$ pairs in the forward region and increase the noice. The average fractional beam energy loss from beamstrahlung is approximately given by [35]:

$$\delta_E \approx 0.86 \frac{r_e^3 N_e^2 \gamma}{\sigma_z (\sigma_x^* + \sigma_y^*)^2} \tag{17}$$

where

Parameter	Symbol	Value
Repetition rate	f_{rep}	5 Hz
Beam pulse length	T_P	950 μs
RF-pulse length	T_{RF}	1370 μs
No. of bunches per pulse	n_b	2820
Bunch spacing	Δt_b	337 ns
Charge per bunch	N_e	2×10^{10}
Beam size at IP	$\sigma^*_{x,y}$	553, 5 nm
Bunch length at IP	σ_z	0.3 mm
Beamstrahlung	δ_E	3.2%
Luminosity	$L_{e^+e^-}$	$\mathbf{3.4 \times 10^{34}\, cm^{-2}s^{-1}}$

Table 1: TESLA beam parameters at 500 GeV operation [27].

r_e the electron classical radius
γ the relativistic factor $E_{beam}/m_e c^2$

The $\sim 1/(\sigma^*_x + \sigma^*_y)^2$ dependence of δ_E allows us to increase L by making the beam highly oblate ($\sigma^*_x \gg \sigma^*_y$). In that limit, σ^*_y becomes insignificant for δ_E, and we can increase L by decreasing σ^*_y as much as possible.

Thanks to the superconducting technology in RF cavities, we can have very high quality accelerating fields, which help to keep the emittance low and give the appropriate shape to the beam. At the TESLA design it is predicted that the beam will have the parameters of table 1, which yield a luminosity of $3.4 \times 10^{34}\, cm^{-2}s^{-1}$. At this luminosity, in a little more than 1 year of operation we will have an integrated luminosity of 1000 fb^{-1}. It is indicative to mention that at LEP stopped working after having collected about 100 pb^{-1} of (on tape) data.

To make the luminosity even higher one would have to alter some of the parameters of the beam. We see that in eq. 16 that $L \propto N_e^2$, so we could increase the luminosity by a factor of 4 by doubling the N_e. To do that we would need to extract electrons at double intensity (double current, using more electron guns if necessary) and send them to the preaccelerator[5]. To double positrons is more complicated, because they are not produced by simple devices such as electron guns. But still, we simply need to produce more photons to convert to e^+e^- pairs. We can increase the current of positrons by increasing the current of electrons that pass through the wiggling magnet, which is as easy as to produce more electrons for the e^- linac. Of course, by changing N_e the optics of the beam will not be the same. It will be harder to focuss and reduce its emittance, because more particles of same charge will be packed in the same volume. But with the installation of more and/or stronger magnets this problem should be resolved.

---

[5]At TESLA the electrons (positrons) will have energy 250 MeV when they enter the damping ring, where they are accelerated to 5 GeV and then enter the linac to reach 250 GeV.

3.3 The detector

This subsection probably should be read after on in parallel with the section describing the physics analysis plan. The reason is that as we determine the analysis we enrich our detector with the instruments it needs to meet the requirements of the analysis and to make its results as accurate as possible.

The key characteristics of our detector, designed for the particular study of the Higgs boson, should be *precision vertexing*, excellent *jets resolution* and *flavor tagging*. The detector needs to combine the following parts:

- The Magnet

- The Tracker

- The Electromagnetic Calorimeter (ECal)

- The Hadronic Calorimeter (HCal)

- The Muon System (MS)

Also, an important part of the detector is the LCAL (luminosity calorimeter) which is used to monitor and fine-tune the luminosity of the beam. It will be located in the inner mask and will be made of tungsten to be able to stand the high radiation environment near the beam. It will be measuring mostly e^+e^- pairs produced by Bhabha scattering and beamstrahlung. In addition, it will be part of the shield that will be protecting the inner tracker from the beamstrahlung radiation. The energy of the beam is expected to be calibrated to the level of 0.1% [27].

One of the sources of noise in almost all experiments is the *cosmic radiation* (CR) reaching the detectors[6]. Blocking charged cosmic particles with magnets would be very difficult because we would need extremely many and powerful magnets to deflect particles of energy up to $\sim 10^{20}$ eV. Neutral particles would feel nothing in the magnetic fields. We would need tones of concrete, which is cheap, to block them. The simplest and probably the only way to shield the detector against cosmic rays is to hide it under a huge amount of matter, usually being the soil and rocks of the Earth. So, that would be rewarding to build *the detector* inside a mountain. Inevitably, due to the size of the basis of mountains, we would have to build at least a great part of the linacs inside the mountain too, in not the whole structure. That would make the project extremely expensive, but it is beyond the scope of this work to worry about its cost. However, we should consider the technical difficulty that appears when we need to build such a huge structure in a mountain. Since we have no budget limitations, that would probably be easier for the engineers to construct the LC

---

[6]This is actually a serious consideretion at low statistics experiments, such as neutrino experiments, where the event rate is so small that CR events would be comparable. But at experiments such as those at Tevatron or at LHC or at the future LC, where the luminosity is huge, CR is a negligible effect. However, I will address it as a problem only for educational reasons.

(and the detector of course) in a valley and after having built it to bring a bulk of matterial and cover the detector (and any part of the linacs they will have to cover).

In addition to the physical shielding of the detector we could possibly apply some clever triggers to exclude events of cosmic radiation. For example, we could build (at least) one hemispherical layer of scintillator around our detector. In this way, we would be able to detect charged high-energy penetrative particles (mainly muons) crossing this shell, by the light they would produce in the scintillator, which we would then collect with optic fibers and convert to electric signals with photomultipliers. Then, by comparing the *time of flight* (TOF) between their passing through the shell and their occurrence in the detector we would be able to say if they were cosmic particles. If the time interval is equal to the time it would take the light to travel from the outer shell to the detector, then we should regard the detected particle as of cosmic origin and exclude the event. This criterion is what we call a *veto* imposition.

3.3.1   The magnet

Let's examine one by one the parts of the detector. We first will determine the properties of the *magnet*. The design of the magnet may follow the general characteristics of the magnet of CMS [36]. A 4 T magnetic field, combined with a high granularity tracker, would be more than enough to give us a good measure of the momentum and charge sign of charged particles (see Appendix). The barrel yoke and the superconducting coil should enclose the tracker, the ECal and the Hcal, as in CMS. One of the reasons is that we would not like the material of the yoke to affect the particles before they reach the calorimeters. The length of the coil should be as long as the horizontal dimension of the detector. It is important to achieve a magnetic field as homogeneous as possible.

3.3.2   The tracker

The *Tracker* is needed for two reasons:

1. To record the tracks that charged particles leave as they come out of the IP. Then we can calculate their transverse momentum p_T (see appendix).

2. To tag secondary vertices, providing a way to identify the flavor of quarks produced close to the IP.

In experiments usually the tracker is separated in two (or more) parts; the inner and the outer tracker. The inner tracker is more finely granular, to be able to give information about the position where a particle decays; this is what we need the inner tracker for. Because of its high granularity the inner tracker is very expensive. The outer tracker is supposed to record the trajectory of charged particles that cross it, and obviously does not need to be as fine granular as the inner tracker. There are three main kinds of trackers:
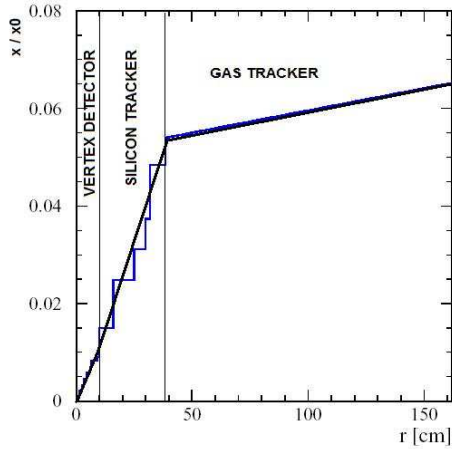
Figure 14: Matter distribution at polar angle $\theta = 90°$ for a tracker consisting of 3 parts: the vertex detector, the silicon tracker and the gas tracker [27].

1. Silicon pixels

2. Gas tracker,

3. Charge-Coupled Devices (CCD)

Since we are not money restricted, we could think that it would be a good idea to fill the whole tracker volume with EBCCDs, as small as $10\,\mu m$, in order to have very accurate tracking of our charged particles. EBCCDs [37] are an improvement of the usual CCDs, in the sense that they amplify the signal reducing the noise which we would have if we used usual CCDs. Of course, by selecting this expensive option, we would have to take care of the Data Acquisition (DAQ) system, since the channels to read out would be extremely many ($\sim 10^{16}$).

In order to avoid this immense number of channels we should apply the method that is applied generally, which is to change the kind of tracker as we go to greater distances from the IP. Actually, even if we had a way to deal with the great number of channels, we would still need to change the kind of tracker at greater distances from the IP, because it is important not to interpose too much material between the IP and the calorimeters, as it would cause absorption by multiple scattering and ionization. One way to do that is to divide the tracker into a Vertex Detector, using EBCCDs, and a Gas Tracker, which will be around the Vertex Detector. We can equip the Gas Tracker with many readout points in the radial direction. For example, in the desing for TESLA, the Gas Tracker is expected to detect ∼200 space points per track. We could increase this number to make the momentum measurement more accurate. The material distribution along the radius r from the IP and at polar angle $\theta = 90°$ is seen in fig. 14 and it's obvious how much density we avoid by using the Gas Tracker instead of filling all the tracker with CCDs.
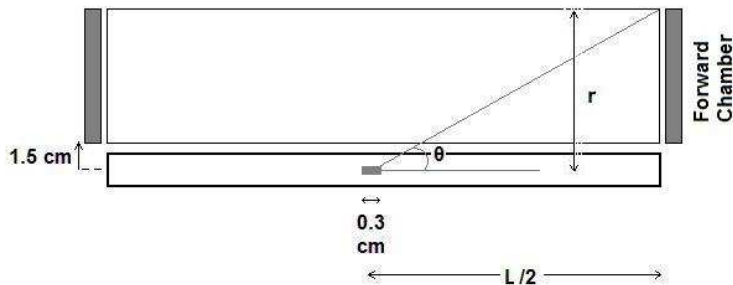
24

Figure 15: Coarse sketch of the size of the tracker and the beam pipe at the IP.

As we calculated in the appendix, an ideal tracker of radius 1.5 m, with uniform spacial resolution of 10 μm would be extremely precise ($\delta(1/p_T) \approx 9 \times 10^{-6}\, GeV^{-1}$). This high p_T resolution in reality will be about $5 \times 10^{-5}\, GeV^{-1}$, which is still very good, and it is achieved by interposing a layer of silicon tracker between the Vertex Detector and the Gas Tracker [27].

As we will see in the according chapter of the analysis plan, we need to observe particles in the forward and backward region of the detector, because the angular distribution of the products of polarized e^+e^- interactions is characteristic at small polar angle (large $|\eta|$). To have a good geometric acceptance we need to determine appropriately the dimensions of the tracker. One of the advantages of a e^+e^- LC is that the beam pipe at the IP can be very narrow (1 cm), allowing the Vertex Detector to get close enough (1.5 cm) to the IP to increase the vertex tagging efficiency. For a tracker of total radius $r = 1.5\,m$, in order to have coverage down to an angle $\theta = 11.5°$ with $\cos\theta = 0.98$ we need the tracker to have length $L = 2 \times \frac{r}{\tan\theta} = 2 \times 7.4\,m$ (see fig. 15).

Apart from making a long enough tracker, we can further improve the track recognition by installing an additional part to the tracker, called *the Forward Chamber*, located right behind the Gas Tracker (see fig. 15). This tracker is a silicon tracker that acts complementarily with the Gas Tracker to provide better momentum resolution and charge sign determination at small polar angles, $\theta < 11.5°$.

There is an issue we should consider, and it is the exposure of the inner tracker (the Vertex Detector mostly) to radiation. This radiation is expected to be dominantly e^+e^- pairs which are produced by high energy photons produced by beamstrahlung. The main bulk of this background is produced in the very forward and backward direction so this is not a serious problem for the greatest part of the detector. Also, the magnetic field of 4 T is strong enough to keep most of this background curling close to the beam pipe. The CCDs at the Vertex Detector, which will mostly suffer from radiation, are easily able to stand radiation of 100krad for a 5 year life.

3.3.3 The Electromagnetic Calorimeter

The next very important part of the detector is the Electromagnetic Calorimeter (ECal), where we measure the energy of electromagnetic showers as well as their shape. It is located around the Tracker and inside the magnetic coil and yoke. One part of it is in the barrel of the detector and another part is in the endcaps, to detect particles at high $|\eta|$. We saw in the appendix that having a tracker of big radius results in better momentum resolution and similarly, having the calorimeters at a bigger distance from the interaction point results in better angular resolution. The radius of 1.5 m combined with a 4 T magnetic field are expected to work sufficiently well.

The characteristics we would like our ECal to combine are:

- Very high granularity in 3 dimensions, which will give us excellent angular resolution and will also allow us to reconstruct the origin of photons hitting the ECal. There are methods, such as neural networks, which can read the parameters of a shower in the ECal (such as its barycentre and spread) and infer whether it is a photon that hit the ECal or two photons coming from a π^0 for example.

- Hermiticity down to small polar angles.

- Good energy resolution, especially *for jets*.

- Fast electronics to have good time resolution, so as to avoid events pile-up.

The ECal needs to have partly absorbing matterial and partly active matterial to detect the products of showers initiated in the absorber layers. A design which would be appropriate for this purpose is a calorimeter with tungsten as an absorber and thin silicon sensors. The silicon and tungsten layers are "sandwiched". The total thickness of tungsten can be selected to be 12 radiation lengths[7]. It is possible to segment transversely the ECal into read-out blocks of area 1 cm^2. It would not make any sense to increase the granularity any further, because the Molière length is about 1 cm, so if the tiles are smaller than that the showers will spread among neighbouring tiles.

At this point I would like to mention that the sampler ("santwich") type of ECal that we selected is not ideal for lepton detection in general[8]. The reason is that as an electron would pass through the successive layers, it would deposit most of its energy in the tungsten plates, leaving only a small part of its energy in the active silicon layers. If about 10% of the electrons energy is deposited in the silicon, then we expect the energy resolution to be approximately: $\Delta E/E \simeq \text{const} + \frac{10\%}{\sqrt{E \times 10\%}}$. We immediately see that the 0.1 factor in the denominator increases ΔE and, even whorse, this 10% is not the same for all electrons and all the times, but it rather fluctuates statistically, which makes the precission of the calorimeter even worse for electrons.

---

[7]Tungsten's radiation length is $X_0 = 3.5\, mm$ and the Molière radius, a measure of the spread of the electromagnetic shower, is about 9 mm.

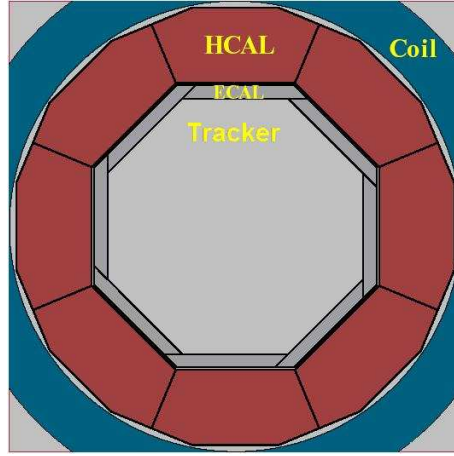[8]As we will explain later, it is good enough in our case.

Figure 16: Drawing of the xy-view of the detector [27].

If we wanted to focus on the precise measurement of electrons and photons then we should have chosen a homogeneous (or "active") detector instead of a layered (or "sampling"). The homogeneous detector is usually made of scintillating crystals, or other kinds of scintillator. The thickness of the crystal should be about or at least 22 radiation lengths, so as not to have any leaking energy[9]. Today there are very dence crystals enriched with Pb and other materials, which make this possible without having to make the ECal extremely thick. The only side-effect of those crystals is the high refraction index that they have ($\eta \approx 3$), which makes it hard to direct the light out of the crystals, due to internal reflections. The way to avoid internal reflections is to use several layers of matterial to join the crystal with the paddle that collects the light and leads it to the optic fibers. Those layers should have gradually reducing η.

In our case the sampler detector would work very well and the reason is the thinness of the tungsten layers. Each one is only $0.4 \times 3.5\,mm = 1.4\,mm$. So, the ECal in this case does not differ so much from a homogeneous one, apart from the fact that it is thinner (228 mm total thickness, 42 mm of which are tungsten) and we do not need to worry about how to collect the light with modified optic fibers, like in the case of dense crystals. Furthermore, we now use silicon instead of scintillating crystal. Silicon is a semiconductor and when an ionizing particle hits it, electron-hole pairs are produced, and a proportional electrical signal is measured. The number of electron-hole pairs that are produced is $n \sim \frac{E_{particle}}{\delta E}$ where δE is the energy required for each pair production. The statistical error in the measurement of n is $\sim \sqrt{n}$ so $\frac{\delta n}{n} \sim \frac{1}{\sqrt{n}}$. This relative error gets very small because of the smallness of δE.

To have very good hermiticity we can use the design of the octagonal ECal shown in fig. 16. Also, in order to have less cracks, we should group the cells of the ECal large modules, whose edges should form cracks which do not point toward the IP. The same care should be paid at the connection of the barrel ECal with the endcap ECal.

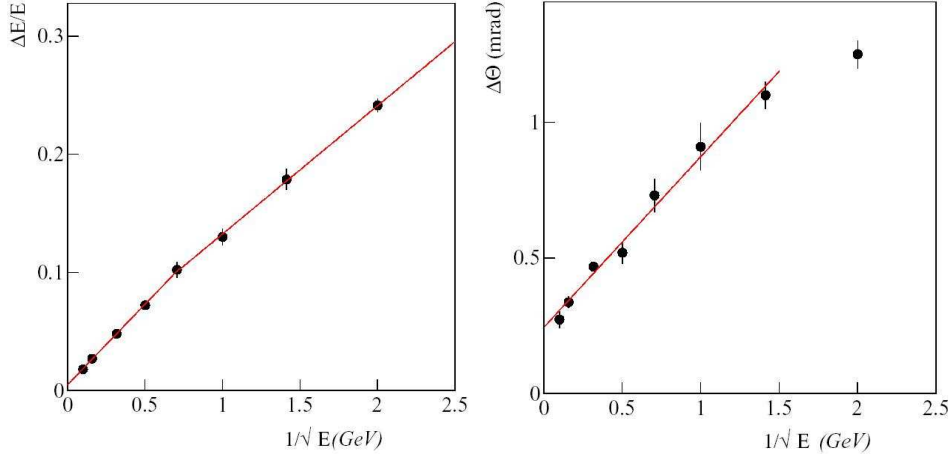[9]How thick it should be also depends on the energy of the electrons, since $E(x) = E_0 e^{-x/X_0}$.

Figure 17: ECal simulated photon energy resolution (left) and angular resolution for photons originating at the primary IP (right) [27].

There is no way to calculate the performance parameters of an ECal without running a simulation, such as those based on GEANT4 [38]. So, I will rely on the simulations run for the design of TESLA [27], which yielded the following specifications:

- Energy resolution $\Delta E/E = 0.11/\sqrt{E}$ in the first energy region and $0.14/\sqrt{E}$ in the second one (see fig. 17).

- Angular resolution of photons originating at the primary IP is about 2 mm for 1 GeV photons and scales $\sim 1/\sqrt{E}$ (see fig. 17).

3.3.4   The Hadronic Calorimeter

The purpose of the Hadronic Calorimeter (HCal) is to work complementarily with the ECal, by detecting the jets which usually penetrate completely the ECal. If some electrons reach the HCal, still it is not too bad.

The principle of operation of the HCal is not any different than that of ECal, especially in the case of an analogue HCal. Again, we can have plates of absorber (such as tungsten or stainless steel) and scintillator (or silicon) and only the size and the cost of the instrument change. It is generally much thicker than the ECal, because its purpose is to contain the whole hadronic shower that will be caused by a jet reaching it. Optic fibers carry the signal out of the scintillator tiles. Those fibers are not simple ones but Wavelength Shifting Fibers (WLS), which are excited by the photons produced in the scintillator and re-emit light at a different frequency. This secondary light can travel without significant energy loss along the WLS fibers and as soon as it reaches the exterior of the detector it is transmitted to "transparent" optic fibers and then to photomultipliers, amplifiers and ADC's to be recorded.

There is also another kind of HCal, the *digital* HCal. It has as active units tiny wire chambers, like ALEPH detector's ECal. Each one of them gives a digital signal (0 or 1) and the number of non-zero signals that are collected is proportional to the energy of the shower in the HCal.

The digital HCal would be a less expensive solution that we would prefer if we had financial restrictions. The next more expensive solution would be an analogue HCal with stainless steel instead of tungsten and scintillator tiles of area $5 \times 5 \, cm^2$ to $25 \times 25 \, cm^2$ at the outer side of the HCal. The thickness of this analogue HCal has been suggested to be $52 \, X_0$. As discussed in [27], the digital HCal can actually have better energy resolution than the – more expensive – analogue HCal.

The ideal – but extremely costly – device would be a HCal of the same granularity and matterial as the ECal, namely made of tungsten and silicon, tiled to the size of $1 \, cm^2$. This is the device we would like to use. The total thickness of tungsten should be again about 52 X_0.

There is no study measuring the performance of such a detector, so we can not say exactly how well it would work. But the study that has been made for the medium-expensive analogue HCal described above has yielded $\Delta E/E \simeq 40\%/\sqrt{E}$ [27]. On the other hand, because of the nature of hadronic and electromagnetic showers, the HCal can not be as precise as $\sim 15\%/\sqrt{E}$, like the ECal. Therefore, I would *estimate* – not completely unjastified – that my HCal would have an energy resolution in the middle of those two values, namely $\Delta E/E \simeq \frac{27\%}{\sqrt{E}}$.

3.3.5   The Muons System

The outer part of the detector should be the muon calorimeter – or muon system –. Muons are extremely penetrative particles, because they do not interact strongly (like jets) and do not bremstrahlung as much as electrons due to their 200 times greater mass. As a consequence, a special device is needed to detect them.

The muon calorimeter is beyond the ECal, the HCal, the magnet's coil and the magnet's yoke. Still, however, a lot of matterial is necessary to absorb the muons that pop out of the magnet's yoke.

In many experiments the muon system is supposed to identify muons and also to measure their momentum with some precision. However, in a e^+e^- LC the events are so clear that tagging a muon at the muon system almost always allows us to associate it with one of the tracks in the tracker and have a measurement of its momentum in this manner.

We should use the technology of Resistive Plate Chambers (RPC)[39], as it combines several advantages:

- The construction of the Muon System is much simpler than if we used other detectors, such as scintillator strips, Plastic Steamer Tubes (PST)[40] or silicon pixels etc.
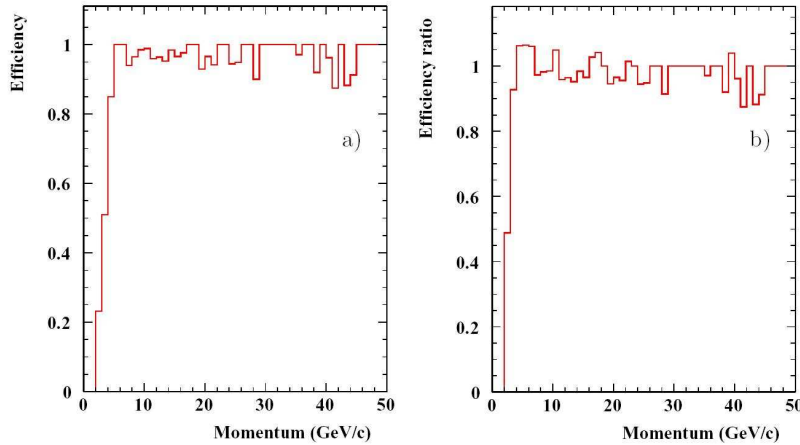
Figure 18: a): Efficiency vs. momentum for $b\bar{b}$ final state. b): Ratio of the $b\bar{b}$ final state muon identification eficiency to single particle identification eficiency.

- Since no wires need to be stretched, their operation does not rely on the 1/R behaviour of the electric field and malfunctioning tends to be confined, unlike the PSTs in which a single non working wire can bring down a larter portion of the detector.

- There is no prefered direction which would possibly make them vulnerable to background.

- RPCs can be shaped almost in any shape, making the detector construction much easier.

The MS should have enough absorber, so a design could include 12 active planes for the barrel, one just in front of the iron, then 10 interspersed in gaps 4cm wide every 10 cm of radiator, with the last one after the last 50 cm of iron. The total thickness of the MS should be about 2 meters. The endcap part of the MS may be of the same structure.

The performance of such a MS has been simulated in the environment of dense $b\bar{b}$ final states [27]. In fig. 18 we see that the efficiency of muon detection is practically 100% and does not get whorse in the environment of $b\bar{b}$ pairs.

Regarding the energy resolution, it will scale as $150\%/\sqrt{E}$ with a constant term of $(20 \pm 10)\%$.

4 Analysis plan

In this section we will describe how measurements at a LC would reveal the existence of the SM Higgs boson and determine its mass.

We will also try to describe a method to observe Higgs decays into a W pair, where W's are either longitudinally or transversely polarized. This measurement would be interesting, because according to the SM, $\sigma_{H^0 \to W_L^+ W_L^-}$ is expected to diverge with increasing center of mass energy ($\sqrt{s}$) as s^2. On the contrary, $\sigma_{H^0 \to W_T^+ W_T^-}$ is finite. Some mechanism must be activated at high energies ($< 1\,TeV$ and about the m_H) to save the unitarity.

4.1 Higgs production and decays

The main mechanisms for the production of Higgs particles in $e^+ e^-$ collisions at energies around 500 GeV are shown in fig. 19. The cross sections for those production modes are compared in fig. 20. We see there that the ZZ fusion is less probable than the other two processes, just because $g_{Zee} < g_{ZWW}$, so we will not use it in our analysis plan.
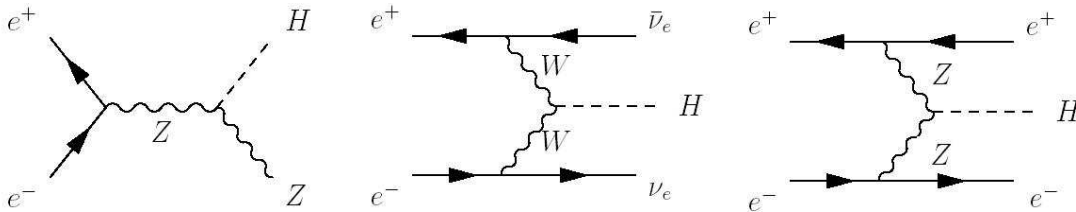

Figure 19: Three main ways Higgs is produced at $\sqrt{s} \approx 500\,GeV$.

By its nature, SM Higgs couples most strongly to the heaviest particles that its mass allows it to decay into. We see in fig. 21 that for a Higgs of mass between 114.4 and 211 GeV, which is the region where the Higgs is most expected to be found, the main decay modes are $W^+ W^-$ and $b\bar{b}$. For heavier Higgs ($m_H > 190\,GeV$), ZZ becomes available and, as Z is much heavier than b-quark, it becomes the second most probable decay mode. For a light Higgs, on the other hand, WW mode is not fully available yet and $b\bar{b}$ is the dominant decay mode.

4.2 Mass analysis

It is possible and rather simple to measure the mass of the Higgs using the $e^+ e^- \to Z^* \to HZ$ process. In this process, usually refered to as *higgstrahlung*, m_H can be determined by detecting the products of the Z and of the H – if they are visible – and reconstructing their invariant masses (see fig. 22). The cross-section of higgstrahlung and WW fusion is [43]:

$$\sigma\left(e^+ e^- \to HZ^0\right) \;=\; \frac{g_{HZZ}^2}{4\pi} \frac{G_F((c_V^e)^2 + (c_A^e)^2)}{96\sqrt{2}s} \beta_{HZ} \frac{\beta_{HZ}^2 + 12 m_Z^2/s}{(1 - m_Z^2/s)^2} \tag{18}$$
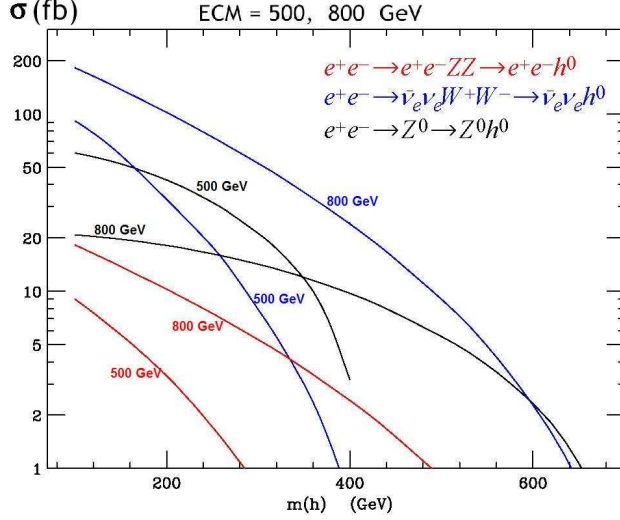
Figure 20: The cross sections of the processes in fig. 19, at 500 and at 800 GeV [41].

$$\sigma\left(e^+e^- \to \bar{\nu}_e\nu_e H\right) = \frac{g^2_{HWW}}{4\pi}\frac{G^2_F}{8\pi^2}\left[\left(1+\frac{m^2_H}{s}\right)\log\frac{s}{m^2_H} - 2\left(1-\frac{m^2_H}{s}\right)\right] \tag{19}$$

where $\beta^2_{ij} = [1 - (m_i + m_j)^2/s][1 - (m_i - m_j)^2/s]$, $c^e_V = -1 + 4\sin^2\theta_W$ and $c^e_A = -1$.

What H can decay into we see in fig. 21, but there is also a scenario where H can decay into an invisible state, such as $H \to \tilde{\chi}_1\bar{\tilde{\chi}}_1$ [44]. The very good property of the $H \to ZH$ channel analysis is that we can measure the recoil energy of the Z even without caring what H decays into and still get a result for m_H, so even if H decays into invisible particles the analysis should work. From the kinematics of the decay of the Z^* with mass $m^* = E_{CM} = \sqrt{s} = 500\,GeV$, we get:

$$m^2_H = m^2_Z + s - 2\sqrt{s}E_Z \tag{20}$$

In fig. 23 we see the plot of relation 20, for $\sqrt{s} = 500$ and 350 GeV. The reason we are also plotting the 350 GeV case is that several analyses have been done for this energy and also to note that the range in which E_Z can vary to comply with the most probable range of m_H is broader at 350 GeV.

The Z decay branching ratios are summarized in table 2. We see that the hadronic channel is dominant, being 20 times more probable than any one of the leptonic channels. However, the leptonic decays have very characteristic signatures that are easy to detect. Electrons and muons leave tracks in the tracker and deposit energy in the EM calorimeter. Muons are very penetrative, reaching the Muon System.
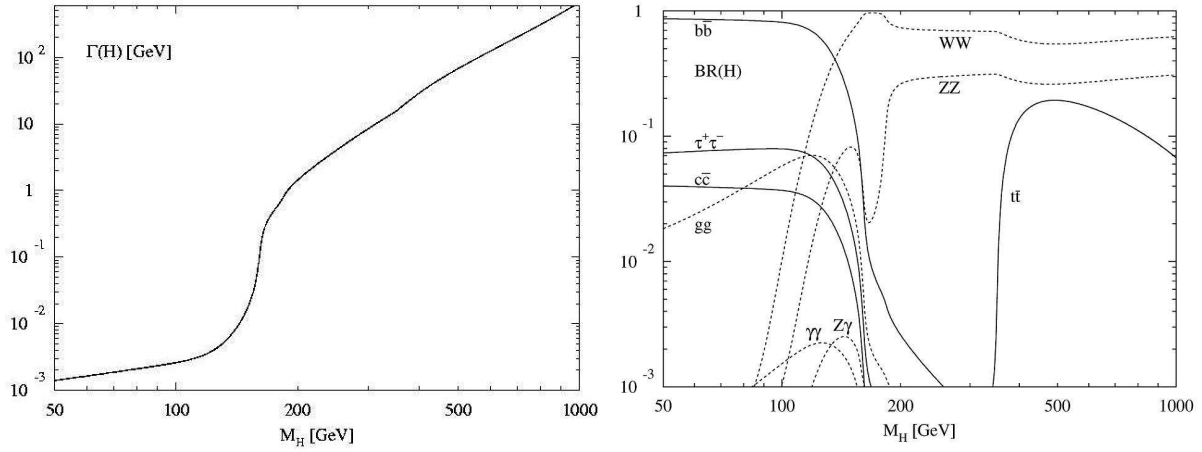
Figure 21: Total decay width $\Gamma(H)$ in GeV and the main branching ratios $BR(H)$ of the Standard Model Higgs decay channels [42].
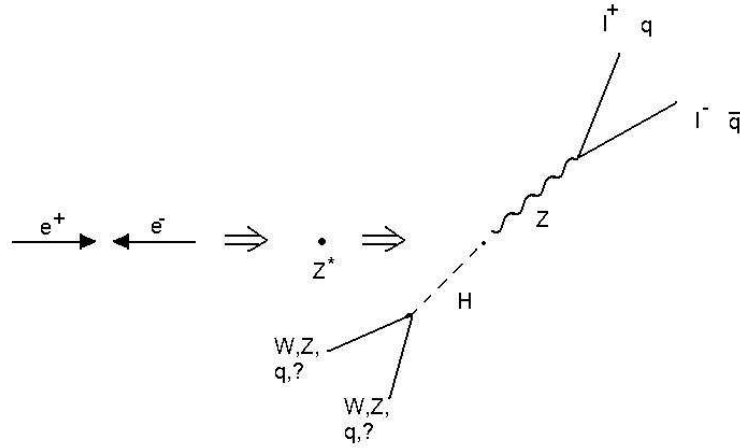

Figure 22: Sketch of a higgstrahlung event.

4.3   The channel $ZH \to e^+e^- + \mathbf{X}$ or $\mu^+\mu^- + \mathbf{X}$

We will rigorously analyse how accurately we could measure the Higgs mass in the channel where the Z decays into an e^+e^- pair and the Higgs goes to anything, including invisible products. The advantage of this channel is that it is very generic, as we are not based on the products of the Higgs. We can make our results more stringent by studying also those products, but we will first see how well we can do without using them.

First of all, we need to recognize the event, and the signature that will allow us to do that combines

- the $\ell^+\ell^-$ pair, which is visible by the track that the charged leptons leave in the tracker and the electromagnetic shower they induce in the ECal and/or the MS, depending on
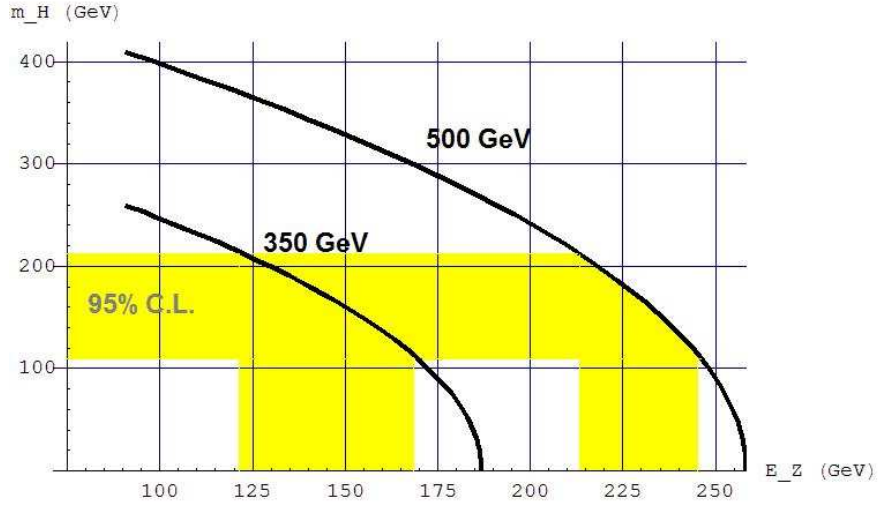
33

Figure 23: Dependence of m_H and E_Z in higgstrahlung for total CM energy of 500 and 350 GeV. Shaded is the range of m_H which is being favored by EW precision measurements, and the corresponding E_Z ranges.

Mode	Fraction Γ_i/Γ
e^+e^-	$(3.363 \pm 0.004)\%$
$\mu^+\mu^-$	$(3.366 \pm 0.007)\%$
$\tau^+\tau^-$	$(3.370 \pm 0.008)\%$
invisible	$(20.00 \pm 0.06)\%$
hadrons	$(69.91 \pm 0.06)\%$
$\mathbf{\Gamma(hadrons)/\Gamma(e^+e^-)}$	$\mathbf{20.804 \pm 0.050}$

Table 2: Z boson brunching rations [45].

whether the leptons are electrons or muons.

- both the ℓ^+ and the ℓ^- start from the same vertex.

- the e^+e^- reconstructed invariant mass equals m_Z. This is the most stringent criterion.

This signal is very clean. The backgrounds are discussed in next section. $Z \to \mu^+\mu^-$ channel *would be much cleaner*, but *the kinematics are the same* since the mass of an electron and a muon are equally negligible compared to the Z mass.

Let's see how accurately the m_H could be reconstructed using *a single*[10] such event. We will use the Tracker for the measurement of the momenta and energies of the produced leptons, as done in the Appendices. From eq. 20, we have:

$$m_H^2 = E_Z^2 - p_{e1}^2 - p_{e2}^2 - 2p_{e1}p_{e2}\cos\Delta\theta + s - 2\sqrt{s}E_Z \Rightarrow \tag{21}$$
$$\delta m_H^2 = \sqrt{T_{12} + T_{21} + T_3 + T_4} \tag{22}$$

where

$$T_{ij} = \left[2\left(p_{ei} + p_{ej}\cos\Delta\theta\right)\delta p_{ei}\right]^2 \tag{23}$$
$$T_3 = \left[2p_{e1}p_{e2}\sin(\Delta\theta)\delta\Delta\theta\right]^2 \tag{24}$$
$$T_4 = \left[2\left(\sqrt{s} - E_Z\right)\delta\sqrt{s}\right]^2 \tag{25}$$

Where $\delta p_{e1,2} = K \times p_{e1,2}^2$. We will also take into account multiple scattering and a granularity induced $\delta\Delta\theta$ (see Appendices). The beam callibration at a collider like TESLA will allow for an uncertainty in the CMS energy of about $\delta\sqrt{s} = 0.1\%\sqrt{s}$. As we will see imidiatelly, the last error is the most important in the accurate measurement of the m_H.

Knowing δm_H^2 and m_H^2 from eq. 20, we calculate

$$\delta m_H = \frac{1}{2\sqrt{m_H^2}}\delta m_H^2 \tag{26}$$

The free parameters that are left to be determined "manually" before making numerical calculations of δm_H are:

E_Z or m_H	correlated through eq. 20. It's more intuitive to use m_H as a parameter
$\theta^* \in [0, 180°]$	the angle of decay of the Z in its rest frame,
$\sqrt{s}$ and $\delta\sqrt{s}$	the collision energy and its error – if not $10^{-3}\sqrt{s}$ –,
G and K	see Appendices. Used values: $10^{-5}\,rad$ and $3 \times 10^{-5}\,GeV^{-1}$

---

[10]Needless to say that high statistics will enhance the accuracy and that is why we don't make measurements with one single observation.
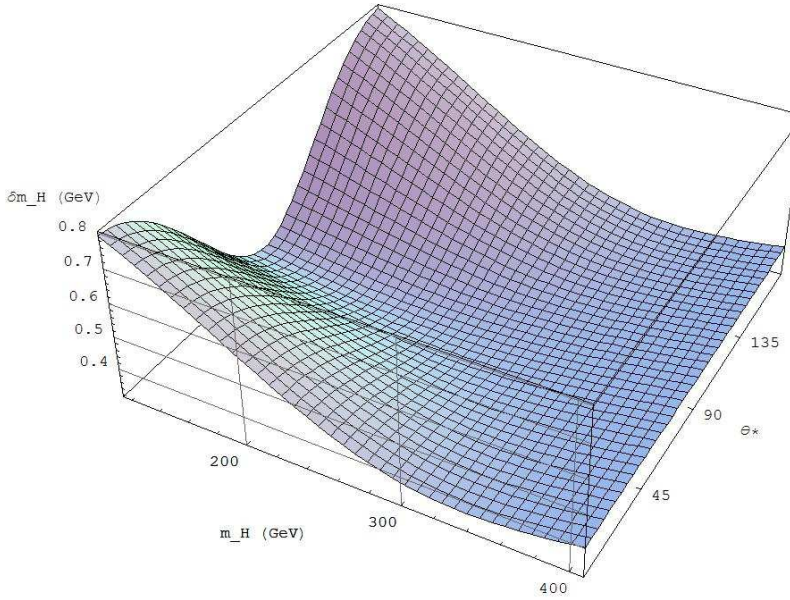
Figure 24: δm_H as a function of m_H and θ^*, for $\sqrt{s} = 500\,GeV \pm 0.1\%$. Plotting $m_H > 114.4\,GeV$.

We will demonstrate first the dependence of δm_H on the collision energy.

Assuming $\sqrt{s} = 500\,GeV$ with 0.1% error, we obtain the δm_H of fig. 24. We see there that it does not exceed 0.8 GeV even in the worst case, of low mass Higgs and Z decaying in the forward-backward direction with respect to its direction of motion. It is probably more informative to plot the profile (projection) of this surface, which we see in fig. 25. The minimum mass error we can get is about 0.31 GeV.

It is interesting to see which the main source of errors is in this channel. To do that, we tampered with the parameter $\delta\sqrt{s}$ and set it equal to zero (0). Then, we obtain the plot in fig. 26.

Technically and quantum-mechanically, it is not possible to eradicate the energy beam error, and 0.1% already quiet good. What about using the accelerator in another energy mode? For a linear collider it would not be so difficult, as it would be for a ring accelerator. The main difference will be just the gradient of the electric field along the linacs. Operating at $\sqrt{s} = 350\,GeV \pm 0.1\%$ would yield the plot in fig. 27. Actually, this performance is better even than then exactly tuned accelerator at 500 GeV. However, there is one serious drawback, and that is the limited range of the m_H that is allowed kinematically.

So, *a recommendable strategy* if we want to use this channel to measure the Higgs mass, would be to start with the LC at 350 GeV, which covers the 114.4-211 GeV region already, and in the case that H is not found there, only then to upgrade the detector to 500 GeV. We see in fig. 25 that in the region $m_H > 260\,GeV$ –beyond the reach of the 350 GeV mode– the accuracy of the 500 GeV mode is very satisfactory ($\delta m_H \leq 0.4\,GeV$).

As a last application of this calculation, let's check how a 1 TeV LC would do in terms of

36

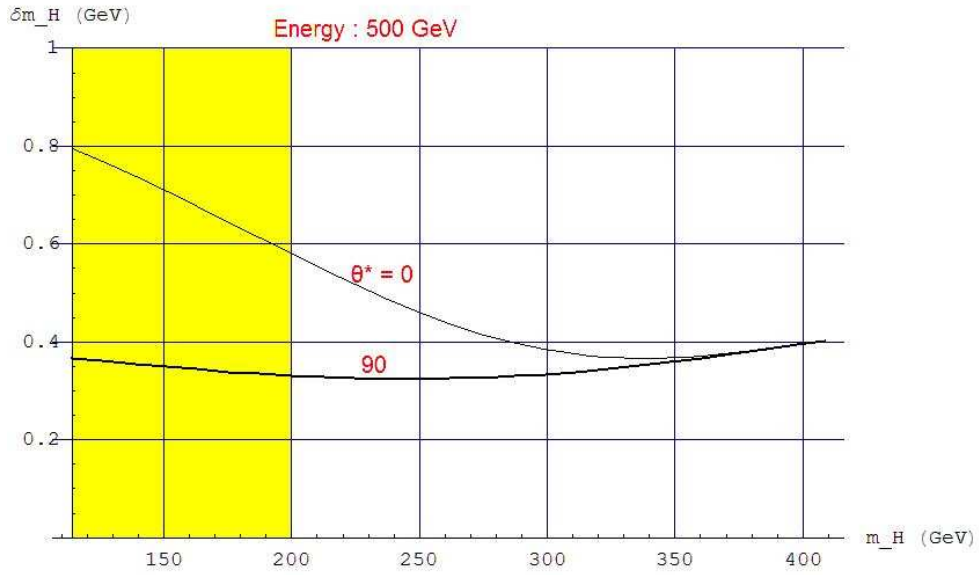Figure 25: δm_H as a function of m_H for $\theta^* = 0$ and $90°$, for $\sqrt{s} = 500\,GeV \pm 0.1\%$. Shaded is the most favored range for m_H.
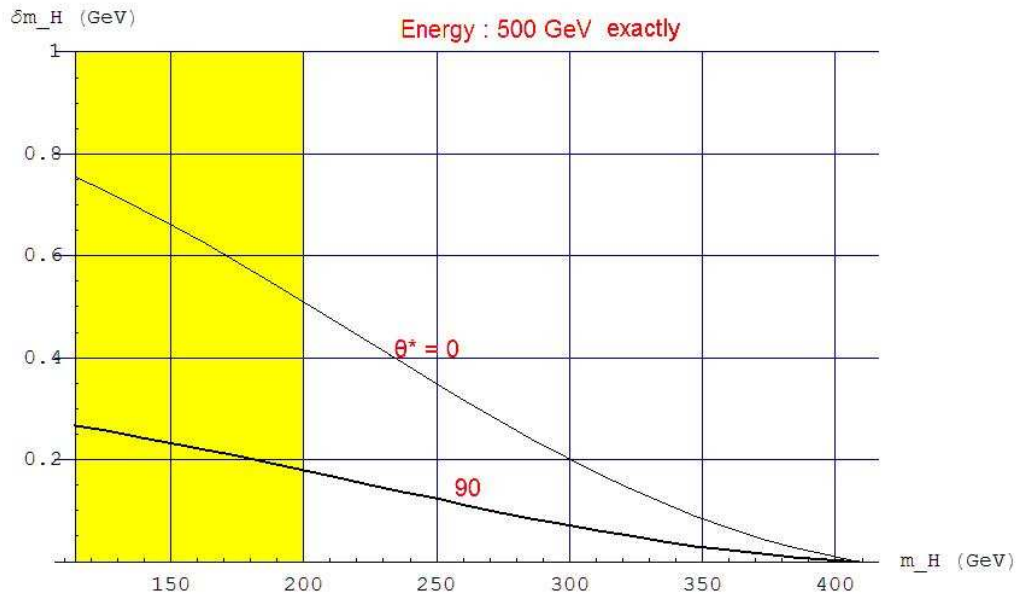

Figure 26: δm_H as a function of m_H for $\theta^* = 0$ and $90°$, for $\sqrt{s} = 500\,GeV \pm 0\%$. Shaded is the most favored range for m_H.
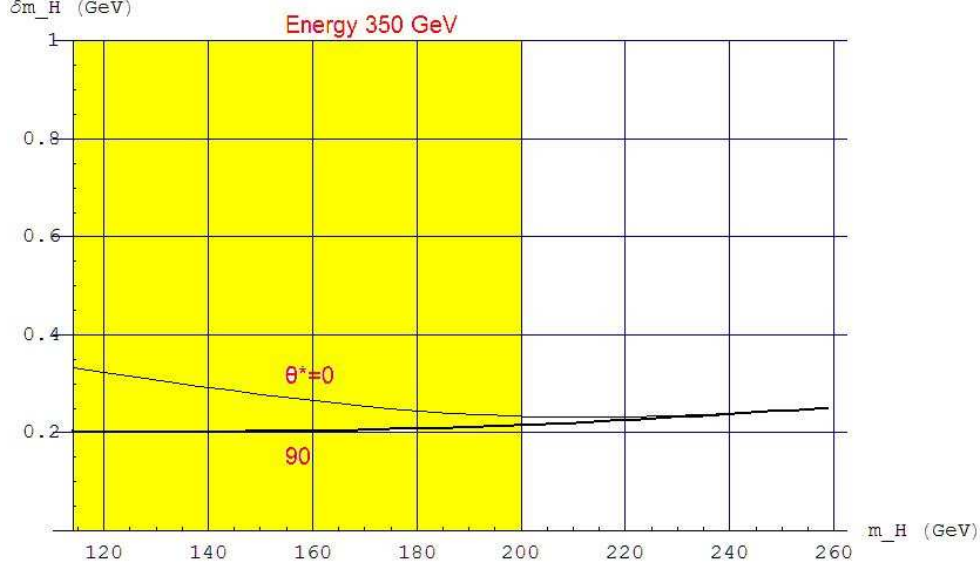
Figure 27: δm_H as a function of m_H for $\theta^* = 0$ and $90°$, for $\sqrt{s} = 350\,GeV \pm 0.1\%$. Shaded is the most favored range for m_H.

δm_H at the channel in examination. We find the plots in fig. 28, which, as expected, show smaller accuracy but great domain of reach, up to $m_H = 908\,GeV$.

To summarize, we calculated so far that the error we will have in *one* measurement of m_H will vary from 0.2GeV to about 0.8 GeV, depending mainly on the m_H, the energy of collision $\sqrt{s}$ and the decay angle θ^* of the Z. The only truly unknown parameter of them is the m_H, because the collision energy we will select (e.g 350 or 500 GeV) and the θ^* can be reconstructed by inverse Lorentz transformation on the Lab-measured momenta of the Z products.

4.3.1   Backgrounds

The major background comes from ZZ, $Z\gamma$ and W^+W^- production (see fig. 10).

Of those background sources, by far the most significant one is the ZZ production. In the 0.06 radiation lengths tracker, the $Z\gamma$ events [51] almost always give a hard photon (trackless energy disposal in the ECal, which neutral networks can distinguish from π^0 mesons). Since the Higgs is not allowed to decay into a single hard photon, we can reject all the events with a hard photon. A W^+W^- pair can result into a $\ell^+\ell^- + \not{E}$ with probability $\sim 0.20 \times 0.10 = 0.02 = 2\%$. But this background becomes negligible after demanding the two leptons to have a reconstructed invariant mass equal to $m_Z \pm 2.5\,GeV$.

But if one of the two Z bosons in a ZZ pair decays leptonically, then the two leptons will of course have the invariant mass of the Z and that event will look like a signal. However, there is a cut that is able to remove most of this background, still without needing to
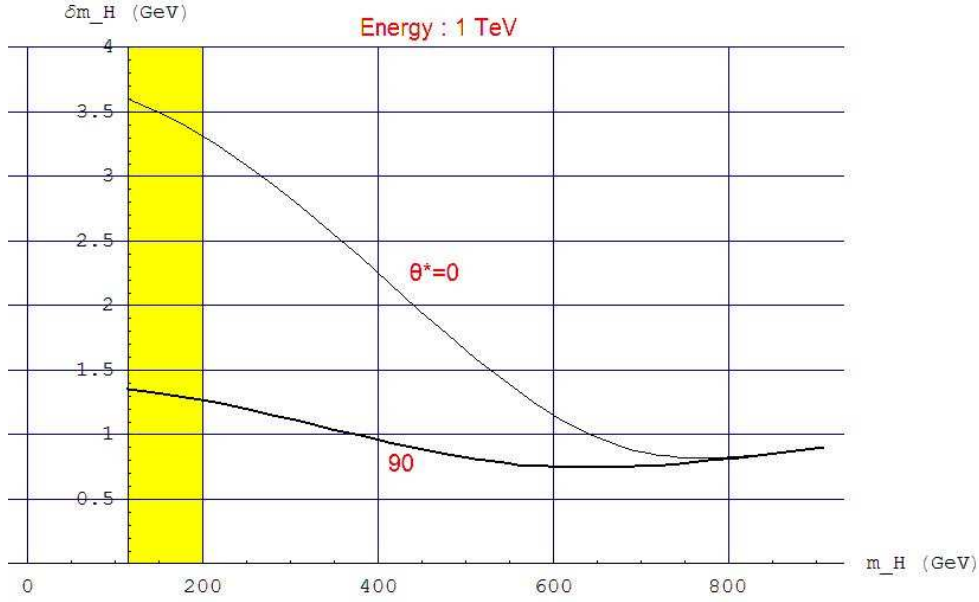
Figure 28: δm_H as a function of m_H for $\theta^* = 0$ and $90°$, for $\sqrt{s} = 1000\,GeV \pm 0.1\%$. Shaded is the most favored range for m_H.

reconstruct the mass of the products of both Z's (or of the Z *and* the H). From eq. 20, by placing m_Z in the place of m_H, we find –as expected– that $E_Z = \sqrt{s}/2$. By inspecting the plot in fig. 23 we see that, at 500 GeV for example, the E_Z of a Z recoiled against the lightest higgs (114.4 GeV) is about 5 GeV smaller than the E_Z of a Z recoiled against another Z (91 GeV). Our resolution in E_Z is much better than 5 GeV, as shown in the Appendices, so we should be able to say the difference of those events, even for the lightest non-excluded H. At smaller energy (350 GeV) the difference gets slightly greater than 5 GeV, namely about 6 GeV. In other words, the mass of the lightest non-excluded Higgs is $114.4 - 91 = 23.4\,GeV$, which is a big difference compared to our resolution in m_H, which has been shown to be less than about 0.8 GeV.

Monte Carlo simulations that have been done [52] using PYTHIA and special detector simulator software, have given interesting results. In fig. 29 we see the characteristic tail of the distribution of the calculated m_H, as give by the simulation. The tail, which expands to the right of the main peak, is due to inefficiency in the measurement of the total of E_Z. We see from eq. 20 that $m_H = \sqrt{m_Z^2 + s - 2\sqrt{s}E_Z}$ so, if only a part of E_Z gets recorded, m_H will seem to be greater than its real (assumed) value.

In fig. 30 we see examples the signal and the background of the $e^+e^- \to ZH \to \ell^+\ell^- X$ channel. All backgrounds have been included, but as we said almost all of it comes from ZZ production. We see that the muonic final state is indeed clearer. In either case, the signal sits on top of a background carpet which decreases at greater values of recoil mass, resembling the tail we saw in fig. 29.

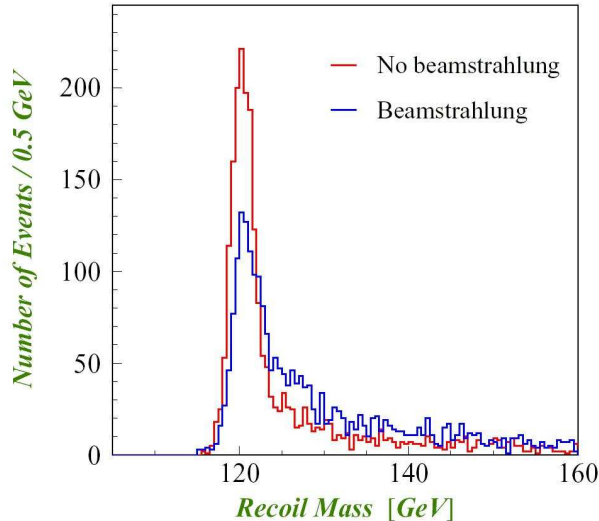The same Monte Carlo simulation has shown that the efficiency for $e^+e^- \to ZH \to \ell^+\ell^- X$

39

Figure 29: The recoil mass spectra off the Z, with and without simulating the beamstrahlung effect. Assumed $\sqrt{s} = 350\,GeV$, sample of $500\,fb^{-1}$ and $m_H = 120\,GeV$ [52].

signal selection is around 50% (see [52] for details).

4.3.2 Higgs Couplings

Though it is not the focal point of my analysis, I would like to refer at this point to the fact that the $ZH \rightarrow e^+e^- + X$ or $\mu^+\mu^- + X$ is also appropriate to study the still unmeasured couplings of the H with its decay products. The way to do that is to tag the higgsstrahlung events in the way we described already, and then identify the products of the Higgs, which will be produced in the oposite direction of the products of the Z. Then, we will be able to measure how frequently the H decays into each of its predicted SM decay modes, hence we will measure the couplings g_{Hbb}, $g_{H\tau\tau}$, g_{Hcc}, g_{HWW}, g_{HZZ} etc. (see fig. 21). A detailed analysis can be found in [49]. If the Higgs is a heavy one, then instead of its couplings to g_{Hbb}, $g_{H\tau\tau}$ and g_{Hcc} we will be able to measure g_{Htt}, which is another very interesting number. Actually, for g_{HWW} and g_{HZZ} we can have much better measurements, because they are associated with the production of the Higgs in the e^+e^- LC (see fig. 19).

What is required for this analysis is to distinguish the processes. To do that, what we need is very good mass resolution and flavor tagging. For a light Higgs b-quark tagging is very important, since most Higgs decay into $b\bar{b}$. At 500 GeV the secondary vertex of the b is expected to have an average displacement of 0.8 cm from the primary vertex, which is more than double the separation we had at LEP[11], making b tagging very efficient. In fig. 31 we see the efficiency and the purity and efficiency of b and c tagging as they were found by

---

[11]At LEP the b decayed about 0.3 cm away from the primary vertex. We can understand why 0.8 cm is reasonable for a 500 GeV e^+e^- collider, if we consider that this is a $\sim$2.5 times bigger energy, so the produced b quarks are expected to have $\sim$2.5 times bigger γ factor, which means 2.5 times longer lifetime.
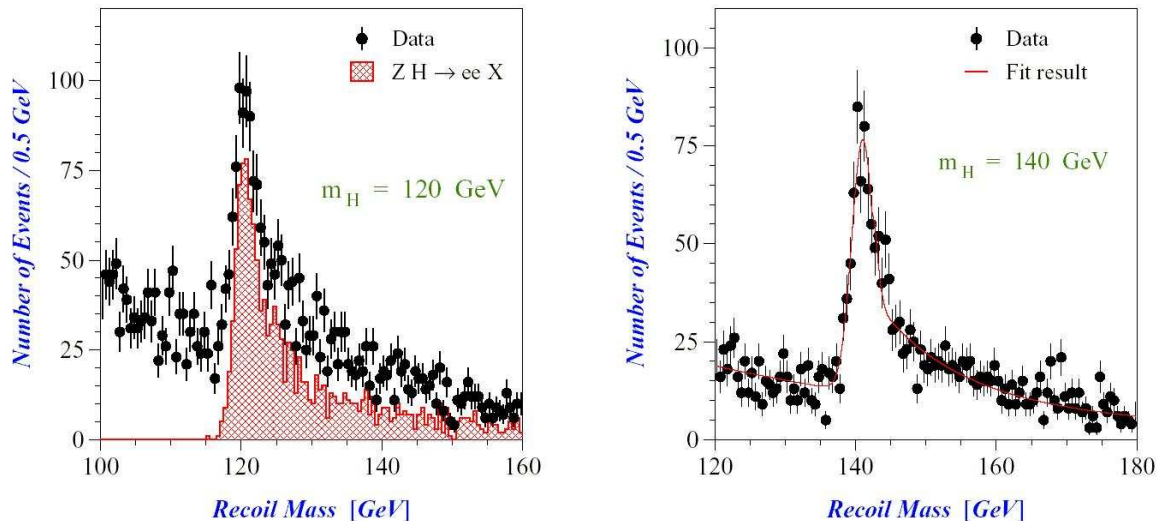
Figure 30: Left: The recoil mass of the Higgs, assuming $m_H = 120\,GeV$ and reconstructing events with $ZH \to e^+e^- X$. Right: The same, assuming $m_H = 140\,GeV$ and using $ZH \to \mu^+\mu^- X$ events. Assumed $\sqrt{s} = 350\,GeV$, sample of $500\,fb^{-1}$ [52].

simulations [48].

Dedicated analysis [49] has shown that the branching rations can be determined at 350 GeV with a $500\ fb^{-1}$ sample to the accuracies presented in fig. 32.

4.4 Optimization and statistics

If we take a great number N of independent measurements of the same quantity x with error $\delta_1 x$, the error δx is reduced as $\frac{\delta_1 x}{\sqrt{N}}$, which is one of the reasons that high statistics is very important in experiments such as this one. The more data we have, the better we know the mass of the Higgs, down to some irreducible systematic error.

I will disregard systematic errors for a moment and look at the expected rate of the several processes (see fig. 20 and table 2). We see that if I run at 500 GeV collision energy and the m_H is bellow 211 GeV, then higgstrahlung has a cross section of about 55 fb. It means that in a data sample of $1000\ fb^{-1}$, which is expected to have been gathered in a little more than one year of running, there will exist 5.5×10^4 higgstrahlung events. By inspecting the branching rations of the Z, we see that $BR(\mu^+\mu^-) = (3.366 \pm 0.007)\%$, so we will have about 1850 events where the Z goes to $\mu^+\mu^-$, which is the cleanest channel. To this very clean sample that one can hardly miss, we can add a percentage of the events that go to e^+e^- and we can tell from the Bhabha background, as well as the events in which $Z \to \tau^+\tau^-$ and our τ tagging efficiency allows us to reconstruct. But even if we do not add those channels to the statistics, and just work with the 1800 clear $\mu^+\mu^-$ events, we will have

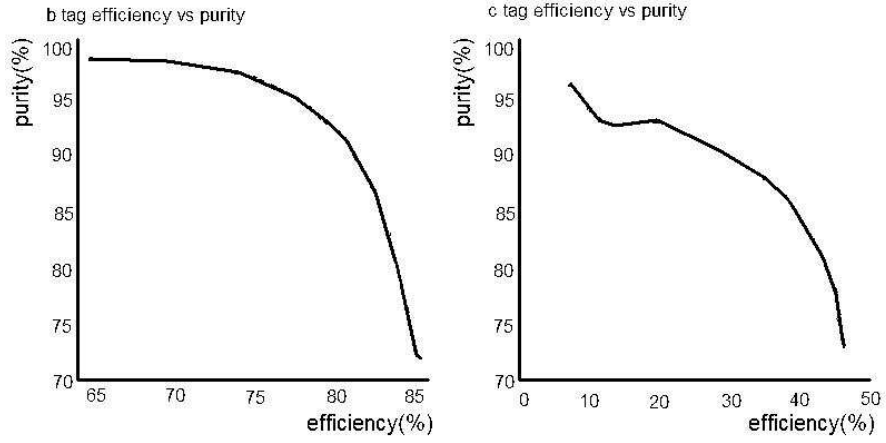$$\delta m_H \simeq \frac{0.5GeV}{\sqrt{1800}} \simeq 12\,MeV \tag{27}$$

41

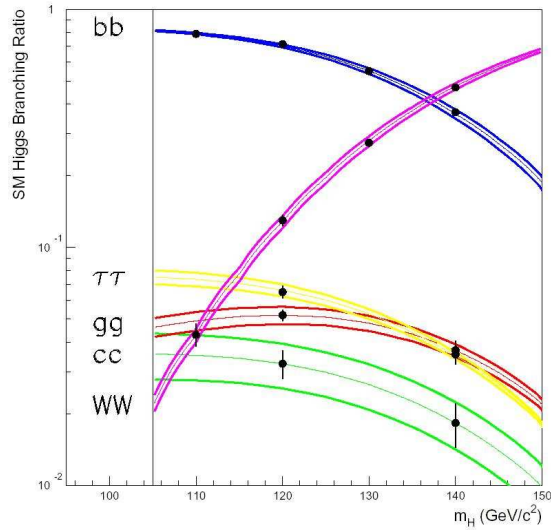Figure 31: Efficiency and purity for b and c tagging [48].

Figure 32: Determination of Higgs boson branching ratios in a variety of decay modes, form [49]. The error bars show the expected experimental errors for 500 fb^{-1} at 350 GeV. The bands show the theoretical errors in the SM predictions [50].

So, a set of $1000\,fb^{-1}$ would reduce our uncertainty of the m_H to the order of $10\,MeV$, if we had no systematic errors at all. TESLA experiment claims to have the possibility to achieve $\delta m_H \approx 60\,MeV$ in a $500\,fb^{-1}$ sample.

Regarding systematic errors, they are a very hard topic which can not be thoroughly analyzed theoretically, because it is 100% related to the hardware of an experiment. What is a systematic error and what is its difference from random errors?

Measuring a quantity which fluctuates randomly would give an outcome that fluctuates equally above and below its mean value by some variance that characterizes how big the uncertainty is. For example, the number of aces that I will have in 100 dice throws fluctuates randomly around the mean value $100/6 = 16.667$. The same is true for measurements of the Z mass. Some times it will be greater than the mean value and some times it will be smaller, in a completely unbiased way.

In contrast to random errors, systematic errors usually come from misscalibration of an instrument. For example, a calorimeter crystal might be faulty and underestimate or overestimate the energy that is deposited in it. Then, we have a biased measurement. Another example could be the energy of the beams. We treated it as a randomly fluctuating quantity of relative uncertainty 0.1%, but in reality it might not be randomly fluctuating but biased. Even whorse, its bias might not be steady over time, but can be affected by seasonal or other time varying effects. For examle, at LEP, by monitoring the beam one could say when a railroad close to CERN was working and when it was not, as it was affecting the instruments causing day-night effects [47].

So, without having all the instruments installed and calibrated, I can not make a good prediction of the systematic errors. That is, in retrospect, the reason that I treated the beam energy uncertainty as a random variance, not as a systematic one.

4.5   LC vs LHC

After all this discussion of the possibilities of Higgs Physics at an e^+e^- LC, this paragraph might be kind of redundant.

At LHC the basic channel to identify the Higgs and measure its mass is the $H \to \gamma\gamma$, which has a very small branching ratio, as shown in fig. 21. Two photon events are not the favorite events of experimentalists, because there are no tracks, and they can be very complicated, with great backgrounds usually. On the other hand, the dominant $b\bar{b}$ final state is useless because of the huge background of jets of all other sources. Only if H is produced in conjunction with a t quark it would be easier to directly observe, because of the characteristic signature of this process.

On the other hand, if nature has selected a heavy Higgs, then there is no doubt that LHC experiments are going to discover it through its $t\bar{t}$, W^+W^- and ZZ decay modes.

If the Higgs is there, it is most probable is that LHC and TEVATRON will give strong signs of it by the time that a LC will be built. But still, LC will be needed after that, because

its great advantages –well known initial energy and particles content, low background, possibly polarized beams– make it necessary for Higgs Precision Measurements. Just discovering the Higgs and measuring its mass is important but is not all about Higgs. We will then need to measure its couplings to all known fermions and bosons, , its self-coupling (the Higgs potential itself), as well as its spin, parity and charge conjucation.

So, most people consider the LC as a project that will work in a complementary fashion with LHC. LHC, with the unprecedented energy of 14 TeV will probe an unknown regime, possibly discovering new particles, proving hypotheses right or wrong. LC, with its precision and simplicity, will then focuss on whatever new is found –including Higgs as a highlight probably– and get into depth in their properties, something LHC could not do.

5   Conclusions

The possiblility of discovering the Higgs boson in a Linear e^+e^- Collider has been investigated. The main advantages of such a collider were discussed; the clarity of the produced events, the high luminosity and good control of the beam, the good knowledge of the initial state, the possibility to change the energy of the beam with relatively simple upgrades. A conceptual design of an appropriate Linear Collider has been presented, including all the states, from the electrons and positrons production to the optimization and control of the beam. A conceptual design of an appropriate detector has also been elaborated, focussing on the details of each part, with the purpose of providing the required instruments for the Higgs mass analysis and for other analyses that such an experiment would allow. An analysis plan has been suggested for the detection of the Higgs and the measurement of its mass. Comments were also made about measuring the couplings of the Higgs and its decay particles. Under the limitation of lack of simulation software, results of other analyses have been used wherever necessary. The greatest portion of the quantitative calculations of this work is included in the Appendices. Starting from first principles, an estimation of the accuracy in the measurement of m_Z and m_H has been made.

The *concluding lines* are that if the Higgs is light we should search for it at 350 GeV collision energy. A 500 GeV LC would be needed if $m_H > 255\,GeV$. The calorimeters should be used for particle identification, while the proposed tracker should be exclusively used to measure momenta –directly– and energies –indirectly–. The mass of the Z can be reconstructed with error $\delta m_Z < 300\,MeV$, allowing perfect Z identification. The mass of the Higgs can be determined down to an error δm_H between 200 and 350 MeV, using a single Higgstrahlung event with a leptonically decaying Z boson. The main background is ZZ production and it is easy to distinguish from the signal, especially in the $ZH \to \mu^+\mu^- X$ channel.

References

[1] D. Abbaneo *et al* [ALEPH, DELPHI, L3 and OPAL Collaborations, LEP Electroweak Working Group, and SLD Heavy Flavour and Electroweak Groups], CERN-EP-2000-016.

[2] A. Straessner, talk given at the XXXVth Rencontres de Moriond (March, 2000).

[3] D. Strom, talk given at the 5th International Symposium on Radiative Corrections (RADCOR-2000), Carmel, CA, 11–15 September, 2000.

[4] Y. Fukuda *et al.* [Super-Kamiokande Collaboration], Phys. Rev. Lett. **81**, 1562 (1998), hep-ex/9807003.

[5] F. Halzen and A.D. Martin: Quarks & Leptons: An Introductory Course in Modern Particle Physics, John Wiley & Sons

[6] Gordon Kane: Modern Elementary Particle Physics, Addison-Wesley

[7] P. Higgs, Phys. Rev. 145 (1966) 1156

[8] E. Farhi and L. Susskind, *Phys. Rep.* **74** (1981) 277; R. K. Kaul, *Rev. Mod. Phys.* **55** (1983) 449; K. Lane, in *The Building Blocks of Creation—From Microfermis to Megaparsecs*, Proceedings of the Theoretical Advanced Study Institute (TASI 93) in Elementary Particle Physics, Boulder, CO, 6 June—2 July 1993, edited by S. Raby and T. Walker (World Scientific, Singapore, 1994).

[9] D.K. Hong, S.D. Hsu, F. Sannino, Composite Higgs from Higher Representations, Phys.Lett. B597 (2004) 89-93, ArXiv:hep-ph/0406200

[10] Nima Arkani-Hamed, Savas Dimopoulos, Supersymmetric Unification Without Low Energy Supersymmetry And Signatures for Fine-Tuning at the LHC, arXiv:hep-th/0405159

[11] Marcela Carena, John S. Conway, Howard E. Haber, John D. Hobbs, Report of the Tevatron Higgs Working Group, arXiv:hep-ph/0010338 v2

[12] Q.S. Yan, D.S. Du, The renormalization of the effective gauge theory with spontaneous symmetry breaking: the $SU(2) \times U(1)$ case, arXiv:hep-ph/0212367

[13] Tarek Ibrahim, Pran Nath, CP Violation in SUSY, Strings and Branes. Invited talk at the Conference on Physics Beyond the Standard Model, Oulu, Finland, 2-7 June, 2002. hep-ph/0207213

[14] J.H. Field, The Experimental Status of the Standard Electroweak Model at the End of the LEP-SLC Era, arXiv:hep-ex/0407040

[15] Degrassi et al [PL B418, 209 (1998)]

[16] Combination of CDF and D Results on W Boson Mass and Width, arXiv:hep-ex/0311039 v2 17 Sep 2004

[17] D. Glenzinski, Measurement of the W Mass from LEP2, hep-ex/9902020

[18] The mass of the W boson, C. Caso, [PL B592, 336 (2004)]

[19] Left-right asymmetries, the weak mixing angle, and new physics, J. C. Montero, V. Pleitez and M. C. Rodriguez, arXiv:hep-ph/0204130 v2 24 Apr 2002

[20] Table of physical constants, [PL B592,(2004)]

[21] Top Quark Mass Measurements at CDF, Pedro A. Movilla Fernandez (on behalf of the CDF Collaboration), arXiv:hep-ex/0409001 v2 5 Nov 2004

[22] Quark Summary Table, [PL B592,(2004)]

[23] STATUS OF THE STRONG COUPLING CONSTANT, Michael Schmelling, arXiv:hep-ex/9701002 v1 9 Jan 1997

[24] Martin W. Grunewald, Electroweak Precision Data Global Higgs Analysis, UCD-EXPH/030401, hep-ex/0304023

[25] S. Choroba for the TESLA Collaboration, THE TESLA RF SYSTEM, http://tdserver1.fnal.gov/8gevlinacPapers/Klystrons_and_HLRF/TESLA_RF_Choroba_MDK2001.pdf

[26] Sun An, SNS Cavity Intrinsic Quality Factor Requirements Based on a Cryomodule Magnetic Shielding Calculation, SNS-NOTE-CRYO-120

[27] The TESLA TDR, http://tesla.desy.de/new_pages/TDR_CD/

[28] V. Sargsyan, Comparison of Stripline and Cavity Beam Position Monitors, TESLA Report 2004-03

[29] David Griffiths, Introduction To Elementary Particles, John Wiley & sons.

[30] A. Miyamoto, in Physics and Experiments with Linear e+e Colliders, F. A. Harris, S. L. Olsen, S. Pakvasa, and X. Tata, eds. (World Scientific, 1993).

[31] M. Woods, The polarized electron beam for the SLAC Linear Collider, SLAC-PUB-7320 October 1996, arXiv:hep-ex/9611006 v1.

[32] Gudrid Moortgat-Pick, Prototype for an undulator-based source for polarised positrons, Eur Phys J C 33, s01, s1047s1050 (2004)

[33] ATF Collaboration, Extremely Low Vertical-Emittance Beam in the Accelerator Test Facility at KEK, VOLUME 88, NUMBER 19 PHYSICAL REVIEW LETTERS 13 MAY 2002.

[34] LHC Design Report,
http://ab-div.web.cern.ch/ab-div/Publications/LHC-DesignReport.html

[35] P. Chen and K. Yokoya, Beam-Beam Phenomena in Linear Colliders, KEK-report 91-2, 1991.

[36] The CMS Technical Proposal.
http://cmsdoc.cern.ch/TPref/TP.html

[37] http://www.syncrotronics.com/New/Frame2.html

[38] http://wwwasd.web.cern.ch/wwwasd/geant4/geant4.html

[39] R. Santonico and R. Cardarelli, Nucl. Instrum. Meth. (A187):377 1981.

[40] E. Iarocci, Proceedings of the International Conference on Instrumentation for Colliding Beam Physics. G. Feldman, editor, Stanford , 1982.

[41] M. Peskin, Higgs Physics at Linear Colliders, lecture presented at FNAL, March 26, 2002.
http://vmsstreamer1.fnal.gov/vms_site_02/Lectures/GSALC02/327Peskin/index.htm

[42] A. Djouadi, J. Kalinowski and M. Spira, HDECAY: a Program for Higgs Boson Decays in the Standard Model and its Supersymmetric Extension, arXiv:hep-ph/9704448 v1 30 Apr 1997

[43] B.W. Lee, C. Quigg, and B. Thacker, Phys. Rev. D16, 1519 (1977).

[44] Ignatios Antoniadis, Marc Tuckmantel, Fabio Zwirner, Phenomenology of a leptonic goldstino and invisible Higgs boson decays, arXiv:hep-ph/0410165

[45] S. Eidelman et al. (Particle Data Group), Phys. Lett. B 592, 1 (2004) (URL: http://pdg.lbl.gov)

[46] J.-C. Brient. LC-PHSM-2000-049
http://www.desy.de/~lcnotes/

[47] Christoph Paus, personal communication.

[48] Rick Van Kooten, Higgs Physics at a Linear Collider, May 3 2001, lecture at FNAL, available at
http://vmsstreamer1.fnal.gov/Lectures/LineDrive/VanKooten/index.htm

[49] Marco Battaglia, Measuring Higgs Branching Ratios and telling the SM from a MSSM Higgs Boson at the e^+e^- Linear Collider, arXiv:hep-ph/9910271 v1 7 Oct 1999

[50] M. Carena and P.M. Zerwas, Higgs Physics, arXiv:hep-ph/9602250 v1 7 Feb 1996

[51] B. Ananthanarayan et al., Transverse beam polarization and CP-violating triple-gauge-boson couplings in $e^+e^- \to Z\gamma$. arXiv:hep-ph/0404106 v1 13 Apr 2004

[52] P. García Abia, W. Lohmann, Measurement of the Higgs Cross Section and Mass with Linear Colliders, arXiv:hep-ex/9908065 v1 30 Aug 1999

[53] Gauge Theory of Weak Interactions, 3rd edition, Greiner & Müller, Springer 2000.

6 Appendices

A Magnetic field, tracker radius, tracker spacial resolution and transverse momentum resolution

In this paragraph of the appendix we will present how the radius of the tracker (r), the magnetic field intensity ($|\vec{B}| = B$), the spacial resolution of the tracker (δs) and the transverse momentum of the particle (p_T) affect the error in the measurement of p_T with the tracker (δp_T). We will assume that the tracker is ideal in the sense that it does not deflect the particle at all from its circular trajectory in the presense of a homogeneus magnetic field B.

A particle of momentum p_T and charge q moves in a circular trajectory of radius R:

$$R = p_T/Bq \Rightarrow RB = \text{rigidity} = p_T/q \tag{28}$$

For example, for electrons of $p_T = 500\,GeV/c$, we have rigidity $RB = \frac{5000}{3}\,T\,m$, which means that if $B = 3\,T$ then $R = 5\,Km$. Only a few meters of that trajectory we are able to record in our tracker of radius r, as shown in fig. 33. The length which we can measure is the distance s, defined as the maximum distance between the curved trajectory in the tracker and the straight line connecting the IP with the point where the particle exits the tracker (see fig. 33).
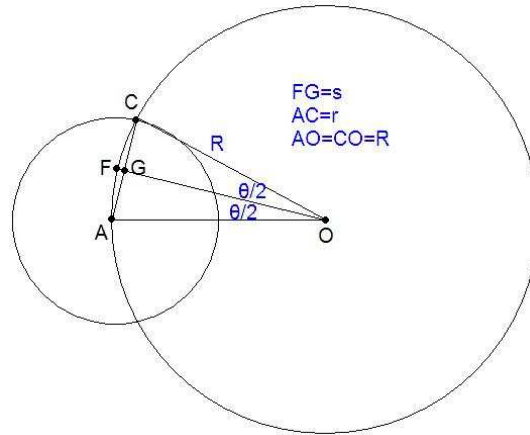

Figure 33: Sketch of the circular trajectory of a particle and of the cross section of the tracker.

After simple geometrical calculations, we see find the formula that correlates r, R and s:
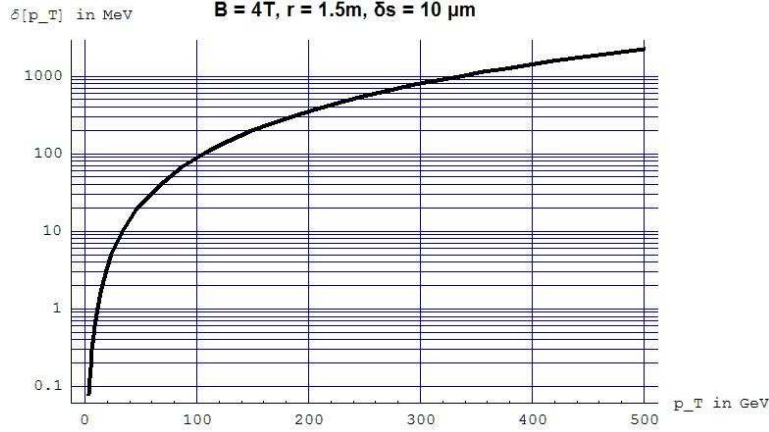
$$s = R - \sqrt{R^2 - \frac{r^2}{2}} \tag{29}$$

Figure 34: δp_T as a function of p_T for an ideal tracker of $r = 1.5\,m$, spacial resolution $\delta s = 10\,\mu m$ and $B = 4\,T$.

Substituting eq. 28 in eq. 29 we get a relationship between s and p_T, r and B, from which we can get:

$$p_T = Bq\frac{\left(\frac{r}{2}\right)^2 + s^2}{2s^2} \tag{30}$$

Assuming no uncertainty in B, we can calculate the error δp_T. If we express s in terms of r, p_T, B and q we acquire the expression:

$$\delta p_T = \delta s \left| Bq - \frac{4p^2}{Bqr^2} - \frac{2p\sqrt{\frac{4p^2}{(Bq)^2} - \frac{r^2}{4}}}{r^2} \right| \tag{31}$$

In fig. 34 we see δp_T as a function of p_T for $r = 1.5\,m$, $B = 4\,T$ and $\delta s = 10\,\mu m$. It is more usual to express the momentum resolution of a tracker as $\delta(1/p_T)$, and this is the quantity plotted in fig. 35. Obviously, a this quantity is almost independent of p_T and allows us to characterize the tracker with a single number, which in this case is $8.9 \times 10^{-6}\,GeV^{-1}$.

B Estimation of the error of momentum using the ideal tracker

In this paragraph we will explain how to calculate the full momentum ($p \equiv |\vec{p}|$) of a charged particle in an (ideal) tracker of finite resolution (δs) and how to estimate its error (δp).

Clearly, the trajectory of the particle is in 3 dimensions, but the curvature of the trajectory projected on the x-y plane gives us only the transverse component of the momentum (p_T) (see fig. 36). The full momentum is given by
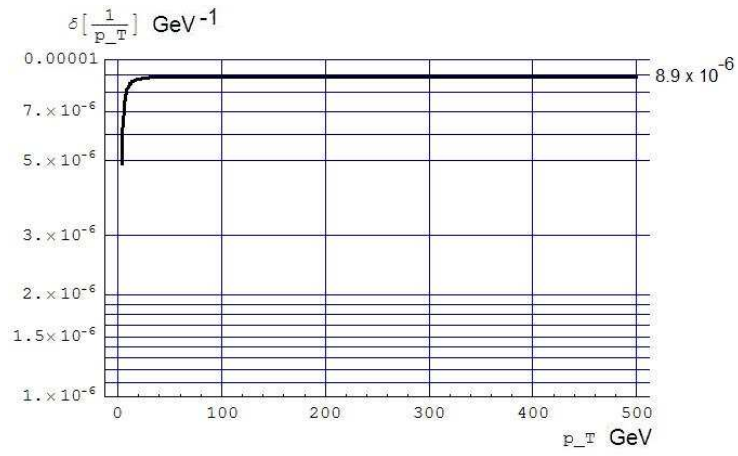
50

Figure 35: $\delta(1/p_T)$ as a function of p_T for an ideal tracker of $r = 1.5\,m$, spacial resolution $\delta s = 10\,\mu m$ and $B = 4\,T$.
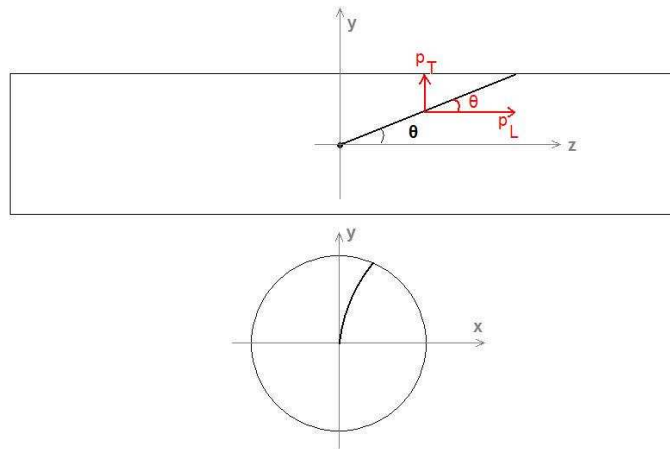

Figure 36: z-y and x-y projection of a track.

51

$$p = \sqrt{p_T^2 + p_L^2} \tag{32}$$

where

$$p_L = \frac{p_T}{\tan \theta} \tag{33}$$

The error in p_L is dependent on δp_T and on $\delta \theta$:

$$
\begin{aligned}
\delta p_L &= \sqrt{\left(\frac{\delta p_T}{\tan \theta}\right)^2 + \left(\frac{p_T}{\tan^2 \theta}\delta(\tan \theta)\right)^2} \\
&= \sqrt{\left(\frac{\delta p_T}{\tan \theta}\right)^2 + \left(\frac{p_T}{\sin^2 \theta}\delta \theta\right)^2}
\end{aligned}
$$

We saw previously that for sufficiently big p_T, $\delta(1/p_T) = \text{const.} \equiv K \Rightarrow \delta p_T = K p_T^2$. So,

$$\delta p_T = \sqrt{\left(\frac{K p_T^2}{\tan \theta}\right)^2 + \left(\frac{p_T}{\sin^2 \theta}\delta \theta\right)^2} \tag{34}$$

Now, the calculation of δp is easy:

$$
\begin{aligned}
\delta p &= \delta\left(\sqrt{p_L^2 + p_T^2}\right) \\
&= \sqrt{\left(\frac{p_L}{p}\delta p_L\right)^2 + \left(\frac{p_T}{p}\delta p_T\right)^2} \\
&= \sqrt{(\cos \theta \delta p_L)^2 + (\sin \theta \delta p_T)^2}
\end{aligned}
$$

After a little algebra, we find:

$$\delta p = K p^2 \sqrt{\cos^4 \theta \sin^2 \theta + \cos^2 \theta (\delta \theta)^2 + \sin^6 \theta} \tag{35}$$

For example, we see that for $\theta = \pi/2$ we have $\delta p = K p^2$, which was expected, since in that case $p = p_T$. For $\theta = 0$ we have $\delta p \propto \delta \theta$, but practically the region of $\theta < 11.5°$ is out of the detector, in the beampipe.

A question that arises is what $\delta \theta$ is. Of course, it is related to the granularity of the tracker; the smaller the pixels the better we can determine the angle of the track with respect to z-axis. It generally depends on more geometrical parameters, including θ, since the tracker is not spherical but cylindrical. For example, if the track starts very close to the end of the tracker and shortly exits it then it's normal to have bigger $\delta \theta$. But since we can not make a Monte Carlo simulation of the tracker, we can just *estimate* $\delta \theta$. It must be on average analogous to $\delta s / S$, where S denotes the characteristic size of the tracker, and we do not distinguish between the length of the tracker and its radius. As we will shortly see, it does not really matter. S can be taken to be of the order of $1\,m$, and δs of the order of $10\,\mu m$. Exaggerating a little, let's say that the average δs may be up to $100\,\mu m$ and S may be as small as 0.1 m. In any case $\delta \theta$ ranges from 10^{-6} rad to 10^{-2}rad $\approx 0.5°$.

In fig. 37 we plot $\delta p / p^2$ as a function of θ, assuming $K = 5 \times 10^{-5}\,GeV^{-1}$, and varying the parameter $\delta \theta$ from 10^{-6} rad to the excessively large value of $15°$. What we see is the very small dependence of this function on $\delta \theta$. We also see that for a specific momentum p, the error δp is maximum at $\theta = 90°$.
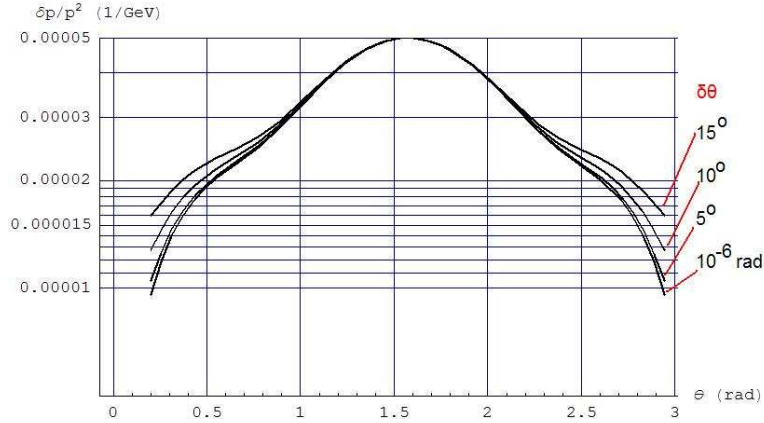
Figure 37: $\delta p / p^2$ as a function of θ, assuming $K = 5 \times 10^{-5} \, GeV^{-1}$, letting the parameter $\delta \theta$ vary from 10^{-6} rad to the excessively large value of $15°$.
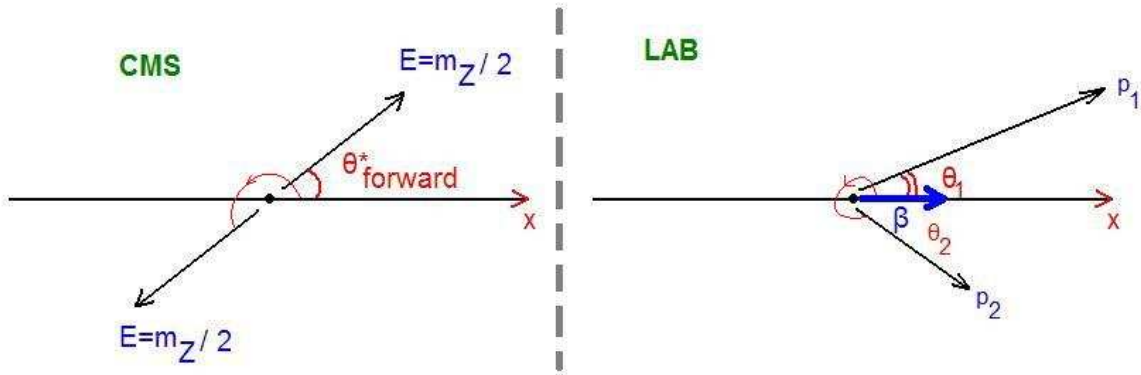

Figure 38: Drawing of the decay of a particle in its CMS and in the Lab system.

C   Angular separation of the decay products of a particle in motion

In the Analysis section we see that it is crucial to be able to detect the product particles of moving particles. For example, the decay products of the Z need to be detected to reconstruct the Z mass and to measure its energy. Sometimes, it is difficult to detect the 2 particles being produced in a decay, because their angular separation can be too small.

In this paragraph of the appendix we are going to solve the kinematic problem of the angular separation of the products of a moving particle.

As an example to work out we will consider the decay of a Z boson into $e^+ e^-$. We define the x-axis in the direction of motion of the Z with respect to the Lab. In the CMS of the Z, the two leptons move back to back. The angles between their momenta and the positive x half axis are θ^* and $\theta^* + \pi$, with θ^* from 0 to π (see fig. 38).
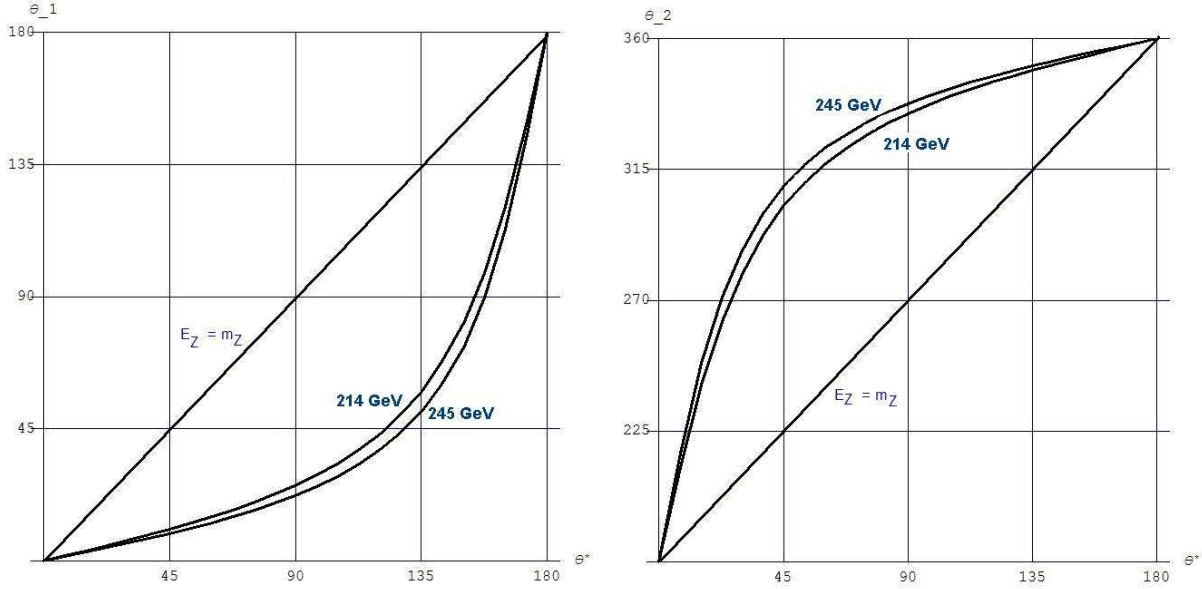
Figure 39: For a Z decaying into a e^+e^- pair *Left*: θ_1 as a function of θ^* and *Right*: θ_2 as a function of θ^*, for Z energy m_Z (at rest), 214 and 245 GeV (see fig. 23). Notice that $\theta_2 > 180°$, in accordance with our definitions.

We know that at the CMS the two leptons have the same energy $E^* = m_Z/2$. For any momentum with components (p_x^*, p_y^*) in the CMS, we can apply a Lorentz transformation to find how it looks in the Lab system (p_x, p_y), where the CMS moves with respect to the Lab at speed $\beta = \sqrt{1 - (1/\gamma)^2} = \sqrt{1 - (m_Z/E_Z)^2}$.

$$p_x = \gamma(p_x^* + \beta E^*) = \gamma(p^* \cos\theta^* + \beta(m_Z/2)) \tag{36}$$
$$p_y = p_y^* = p \sin\theta^* \tag{37}$$

From the relations 36 and 37 we can calculate the angle θ of the momentum in the lab:

$$\tan\theta = \frac{py}{px} = \frac{\sin\theta^*}{\frac{E_Z}{m_Z}\left[\cos\theta^* + \beta\sqrt{\frac{m_Z^2}{m_Z^2 - 4m_\ell^2}}\right]} \tag{38}$$

Now, we can apply this formula to transform independently $\theta^* \to \theta_1$ and $\theta^* + \pi \to \theta_2$. Giving to the lepton the mass of an electron and to the decaying particle the mass of Z boson, we get the plots in fig. 39.

Since we have the two angles, it is easy to plot the separation of the two product particles in the Lab system (see fig. 40). From this plot we clearly see that for a decaying Z of the energy that we expect to have at a 500 GeV LC, the products will never be closer than 45° in θ. This is true for a Z decaying into a pair of much lighter particles, such as all the leptons and all the quarks Z can decay into[12].

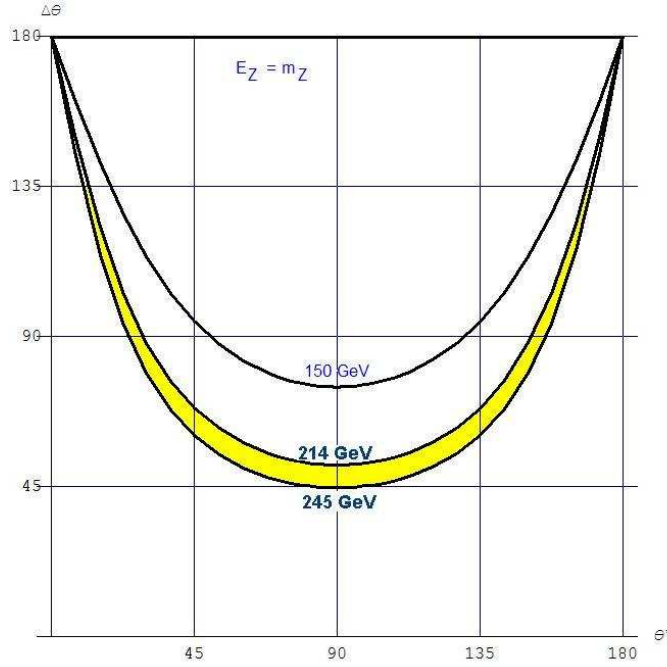[12] Even for $b\bar{b}$ of mass 4.4 GeV the kinematics remains practically the same.

Figure 40: Separation in θ of the products of a decaying Z, as a function of θ^*, for several Z energies.

The kinematics of $H \rightarrow W^+W^-$, to take another example, is very different, because of the big mass of W compared to a H, which we will assume to be 200 GeV. The basic difference is that the separation can now be close to zero, if two conditions are satisfied: 1) The θ^* has to be close to 0 or to π, and the energy of the H has to be above a critical level. This level, generally is

$$E^{cr}_{\text{Parent Particle}} = \frac{1}{2} \frac{m^2_{\text{Parent Particle}}}{m_{\text{Daughter Particle}}} \tag{39}$$

For the $H \rightarrow W^+W^-$, eq. 39 returns $E^{cr}_H \simeq 250\,GeV$, which agrees with what we see in fig. 41.

D   Calculation of the invariant mass of Z and its error

We will work the example of a Z decaying into two electrons. We can tag the e^+e^- using the shape of their showers in the ECal, the lack of energy deposition in the HCAL, the track and the lack of any secondary vertices – except for a production vertex which is where the moving Z decayed –. I need to find the invariant mass of every pair of e^+e^- to check if it is close to the mass of the Z, so as to identify them products of a Z decay.
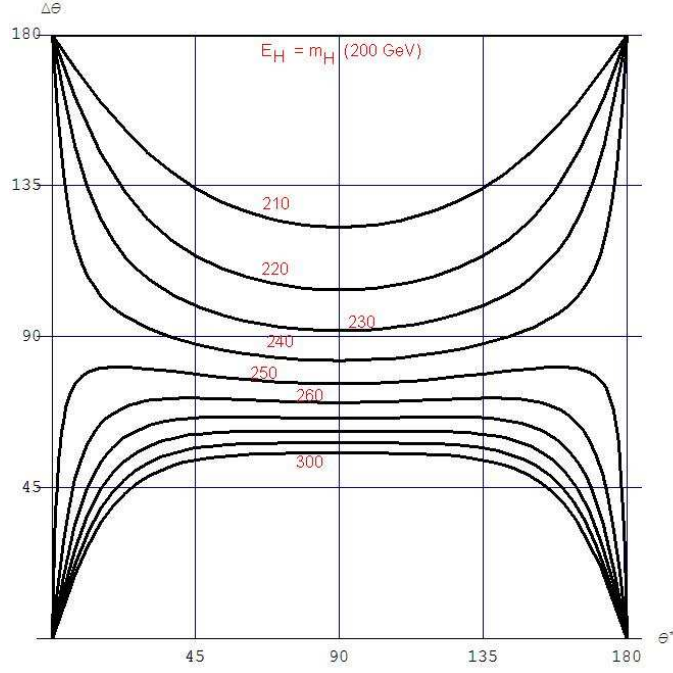
55

Figure 41: Separation in θ of the W^+W^- produced by a decaying H, as a function of θ^*, for several H energies.

The invariant mass of the e^+e^- is easy to calculate:

$$
\begin{aligned}
m_{Inv}^2 &= (E_{e1} + E_{e2})^2 - (\vec{p}_{e1} + \vec{p}_{e2})^2 \\
&= (E_{e1} + E_{e2})^2 - p_{e1}^2 - p_{e2}^2 - 2p_{e1}p_{e2}cos(\Delta\theta)
\end{aligned}
\tag{40}
$$

Where $\Delta\theta$ is the angle between their momentum vectors in the Lab frame. We can measure this angle in the tracker with some error $\delta\Delta\theta$.

In the experiment we will be trying to calculate E_Z and m_Z from what we measure (see eq. 20). The things that we will measure are: the momenta $p_{e1,2}$, the energies they deposit in the ECal $E_{e1,2}$ and the angle $\Delta\theta$. Now I would like to make some calculations to *estimate* the outcomes of those measurements, and my final purpose is to *estimate* the uncertainty I will have in the calculation of m_{Inv}, which will be δm_{Inv}.

As we did in the previous section of the Appendix, given the mass of the Z (m_Z), the mass of the electron (m_e), the energy of the Z ($E_Z \geq m_Z$), and the angle θ^* at which the Z decays in its rest frame, it is possible to calculate the $\Delta\theta$ in eq. 40, as well as the momenta p_{e1} and p_{e2}. Of course, by Lorentz transformation we also have the energies E_{e1} and E_{e2}:

$$
E_{e1} = \gamma\left(\frac{m_Z}{2} + \beta\cos\theta^*\sqrt{(\frac{m_Z}{2})^2 - m_e^2}\right)
\tag{41}
$$

$$
E_{e2} = \gamma\left(\frac{m_Z}{2} + \beta\cos(\theta^* + \pi)\sqrt{(\frac{m_Z}{2})^2 - m_e^2}\right)
\tag{42}
$$

$$
E_{e1} + E_{e2} = E_Z
$$

where $\gamma = \sqrt{\frac{1}{1-\beta^2}} = E_Z/m_Z$.

So, given the E_Z and θ^* I can *go backwards* and calculate analytically the values of the quantities I will measure, as well as their errors. All I have as *free parameters* are the E_Z and the angle $\theta^* \in [0, 180°]$. For example, I already calculated $\Delta\theta$ and I saw that it will be greater than 45 degrees for $E_Z < 245$ GeV and for all U's.

Our purpose is to estimate:

$$\delta m_{Inv} = \delta\sqrt{m_{Inv}^2} = \frac{1}{2\sqrt{m_{Inv}^2}}\delta m_{Inv}^2 \tag{43}$$

From eq. 40 we have:

$$\delta m_{Inv}^2 = 2\sqrt{T1 + T2 + T3 + T4 + T5} \tag{44}$$

where

$$
\begin{aligned}
T1 &= [(E_{e1} + E_{e2})\delta E_{e1}]^2 & (45) \\
T2 &= [(E_{e1} + E_{e2})\delta E_{e2}]^2 & (46) \\
T3 &= [(p_{e1} + p_{e2}\cos\Delta\theta)\delta p_{e1}]^2 & (47) \\
T4 &= [(p_{e2} + p_{e1}\cos\Delta\theta)\delta p_{e2}]^2 & (48) \\
T5 &= [p_{e1}p_{e2}\sin(\Delta\theta)\delta\Delta\theta]^2 & (49)
\end{aligned}
$$

In this equation I substitute equations 41, 42 and $p_{e1,2} = \sqrt{E_{e1,2}^2 - m_e^2}$. I also use eq. 38 to calculate each angle separately and then their difference $\Delta\theta$, as I did in the previous paragraph of thie Appenices (see fig. 40).

After all those substitutions I finally have an expression for δm_{Inv}^2 which depends on the following variables: E_Z, θ^*, m_Z, m_e, $\delta p_{e1,2}$, $\delta\Delta\theta$, $\delta E_{e1,2}$. Of them, the first two are left as free parameters to the end, and the m_Z and m_e are fixed numbers. So, the next step will be to find analytic expressions for the errors $\delta p_{e1,2}$, $\delta\Delta\theta$, $\delta E_{e1,2}$.

From fig. 37[13] and the calculations which lead to that plot, we see that $\delta p_{e1,2}$ is for all polar angles θ smaller than the characteristic parameter of the tracker K which we have previously defined as $\delta(1/p_T)$ and in the experiment will be about $5 \times 10^{-5}\,GeV^{-1}$. Thus, we can *estimate* that

$$\delta p_{e1,2} \simeq (3/5)Kp_{e1,2}^2, \tag{50}$$

by averaging $\delta p/p^2$ over the polar angles $\theta \in [\arccos(0.98), \pi - \arccos(0.98)]$.

As discussed in Appendix B, the accuracy of angles measurement is limited because of the finite granularity and size of our tracker. We justified with some semi-qualitative arguments that for an ideal tracker the resolution in angle is about 10^{-5} rad, so the error in $\Delta\theta$ should

---

[13]Notice that θ in fig. 37 is the polar angle of the track with respect to the beampipe (see fig. 36), and has nothing to do with the angle of a lepton with respect to the direction of motion of its decaying parent Z.

be approximately $\sqrt{2} \times 10^{-5}$ rad. Finally, as we saw in Appendix B and as we will see again here, this resolution does not affect severly the final errors, even if $\delta\Delta\theta$ is several degrees big. So, to summarize, we will *estimate* $\delta\Delta\theta$ as a fixed value of the order of 10^{-5} rad.

We have so far eliminated the factors $\delta p_{e1,2}$ with K and $\delta\Delta\theta$ with a fixed value. What is still remaining is to eliminate $\delta E_{e1,2}$. This uncertainty depends on how we want to determine the energy of an electron or positron. There are two ways to do that:

1. Using the ECal. Then $\delta E_{e1,2} = 0.11 \times \sqrt{E_{e1,2}}$ (I neglect the constant term of the calorimeter) (see fig. 17).

2. Using the information from the tracker. The tracker gives me the momentum and, combined with the ECal, helps me identify which particles are electrons and positrons. Then, knowing the momentum, I calculate the energy of the leptons with some error dependent on the resolution of the tracker as we will see.

D.1 1st approach: Using the ECal

If I use the ECal then
$$\delta E_{e1,2} = 0.11 \times \sqrt{E_{e1,2}} \tag{51}$$
With this assumption, I make all the substitutions and calculations already described and I obtain the plot in fig. 42.
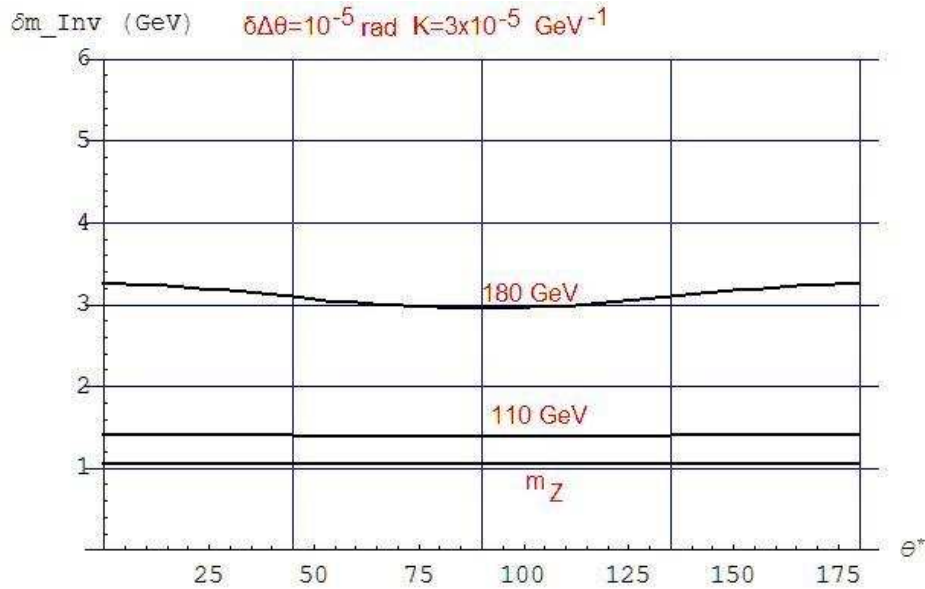

Figure 42: δm_{Inv} of a pair of e^+e^- from a decaying Z, as a function of the parameter θ^* and for three different energies of the Z. Assumed $K = 3 \times 10^{-5}\,GeV^{-1}$ and $\delta\Delta\theta = 10^{-5}\,rad$.

Since θ^* is a parameter I do not know in my effort to go backward and estimate δm_{Inv}, I average δm_{Inv} over all θ^* and I obtain the plot in fig. 43. We see there that the mean δm_{Inv} over all possible θ^* is quiet low in the regime of $E_Z \leq 245\,GeV$.
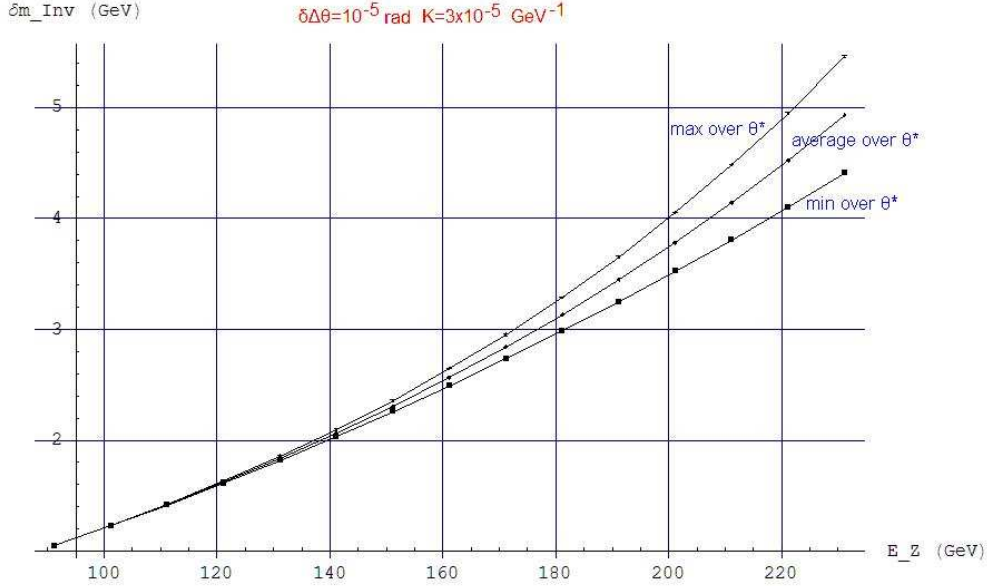

Figure 43: δm_{Inv} averaged over θ^*, surrounded by the minimum and maximum values it takes for varying θ^*, as a function of E_Z. Assumed $K = 3 \times 10^{-5}\,GeV^{-1}$ and $\delta\Delta\theta = 10^{-5}\,rad$.

To demonstrate the weak dependence of this result on $\delta\Delta\theta$, we calculated the same quantities assuming $\delta\Delta\theta = 0.5°$ (!), which is 872 times greater than 10^{-5} rad (see fig. 44).

D.2 2nd approach: Using the Tracker

To use only the momentum measurement to determine $E_{e1,2}$, we have to use the relationship:

$$E_e = \sqrt{p_e^2 + m_e^2},$$

which means simply that the E_e and p_e are 100% *correlated*. We can make use of this correlation and express m_{Inv}^2 only as a function of $p_{e1,2}$:

$$m_{Inv}^2 = 2m_e^2 + 2\sqrt{(m_e^2 + p_{e1}^2) \times (m_e^2 + p_{e2}^2)} - 2p_{e1}p_{e2}\cos\Delta\theta \Rightarrow \tag{52}$$

$$\delta m_{Inv}^2 = \sqrt{T_{12} + T_{21} + 4T_5} \tag{53}$$

where

$$T_{ij} \equiv \left[\left(2\sqrt{m_e^2 + p_{ej}^2}\frac{p_{ei}}{\sqrt{m_e^2 + p_{ei}^2}} - 2p_{ej}\cos\Delta\theta\right)\delta p_{ei}\right]^2 \tag{54}$$
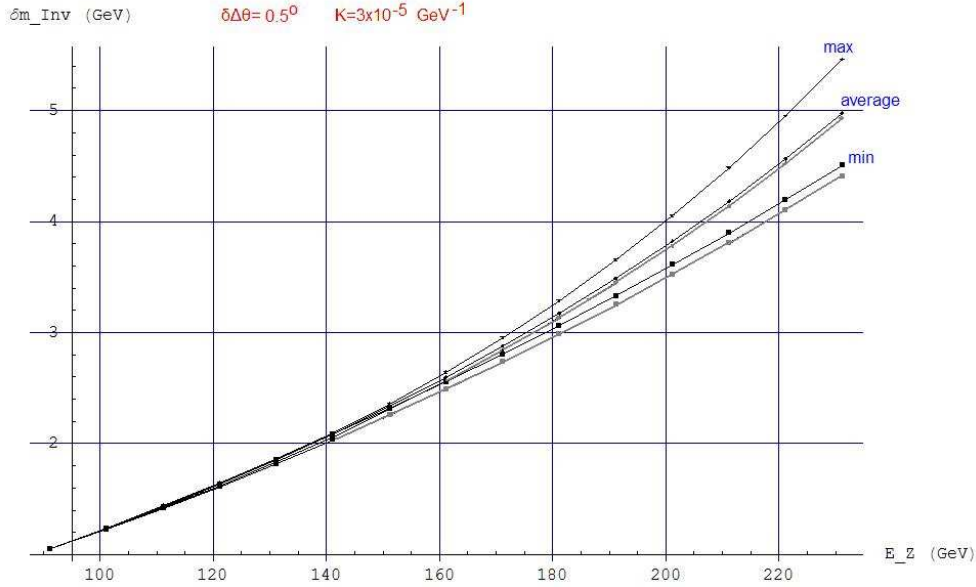
Figure 44: The same as fig. 43, assumed $K = 3 \times 10^{-5}\, GeV^{-1}$ and $\delta\Delta\theta = 0.5°$. The gray line stands where those curves were for $\delta\Delta\theta = 10^{-5}\, \text{rad}$.

Then, $\delta p_{e1,2}$ is given by eq. 50 and $p_{e1,2} = \sqrt{E_{e1,2}^2 - m_e^2}$, where $E_{e1,2}$ is calculated with eq. 41 and 42.

The resulting plots can be seen in fig. 45, 46 and 47. Comparing those results with the results we got using the ECal instead of the Tracker, we realize that the 2nd approach is by a whole order of magnitude more accurate than the 1st one. However, its accuracy is more strongly dependent on $\delta\Delta\theta$, but even for an angular resolution of 0.5° the tracker is much better than the ECal.

D.3   A comment about multiple scattering and $\delta\Delta\theta$

In my treatment so far I have been using $\delta\Delta\theta \sim 10^{-5}\, rad$. This value –or order of magnitude to be exact– was justified semi-qualitatively in Appendix B. But there is a more rigorous way to calculate the error in $\Delta\theta$, taking into account **multiple scattering**.

The formula which gives *the deflection* of an ionizing particle of momentum p, after it has crossed a bulk of matter of thickness ℓ radiation lengths is:

$$D\theta = (15 \times 10^{-3}\, rad)\frac{1}{p_{(GeV)}}\sqrt{\ell} \tag{55}$$

So far, I have been treating the momenta of the decay products as always lying in the same plane, from the beginning to the end of the tracks. Equivalently, I have been assuming that the tracks define a single plane and 'live' in it, as 2-dimensional objects. This is not
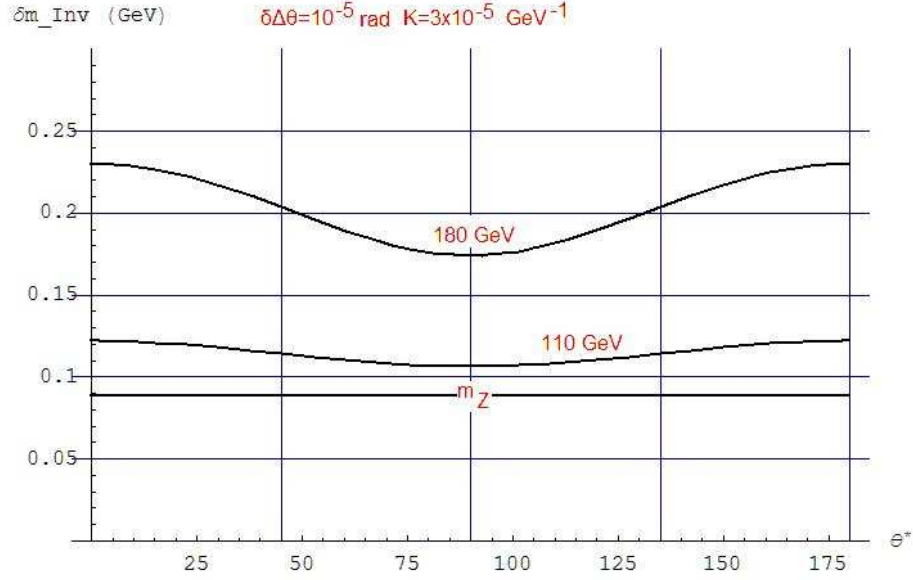
60

Figure 45: The same as fig. 42, but using the Tracker for the determination of the letpons' energy. Tracker gives us an order of magnitude smaller δm_{Inv} than the ECal alone.

quiet true. Multiple scattering makes the momenta deflect in 3 dimensions inside the tracker and the whole track in not a curve in a plane, but in space. However, because of the great complexity of the exact treatment and of time limitations, I will keep assuming that the tracks are planar, hoping that this approximation is not severely wrong.

Therefore, the error in the angular separation $\Delta\theta = \theta_1 - \theta_2$ is written:

$$
\begin{aligned}
\delta\Delta\theta &= \sqrt{(D\theta_1)^2 + (D\theta_2)^2} \\
&= 15 \times 10^{-3}\sqrt{\ell}\sqrt{p_1^{-2} + p_2^{-2}} \; rad
\end{aligned}
\tag{56}
$$

Having this relationship in hand we can substitute it from the beginning in eq. 49. Then, all the calculations remain the same, appart from the fact that now $\delta\Delta\theta$ is not set "by hand" equal to a number, but is eliminated and in its place we have an expression of $p_{e1,2}$.

But let's examine what this relation gives us. Our tracker is expected to have a total thickness of $\ell = 0.06 \, X_0$ (see fig. 14). For a decaying Z, the momentum of an electron in the Lab reference frame may vary significantly, depending on the angle θ^* in which the Z decays (in its own rest frame) and on E_Z. We can easily calculate the $\sqrt{p_1^{-2} + p_2^{-2}}$ factor and, as we see in fig. 48, it never exceeds 0.12 for $E_Z \in [m_Z, 250\,GeV]$. This means that this factor lowers $\delta\Delta\theta$ by one or two orders of magnitude (most usually by two). On the other hand, $\sqrt{\ell} = \sqrt{0.06} = 0.245$ lowers $\delta\Delta\theta$ by another order of magnitude.

So, $\delta\Delta\theta$ as given in eq. 56 is of the order of $10^{-5}\,rad$, which is actually the same order of magnitude we had assigned to it so far. That is the reason that the magnitude of δm_{Inv} that we get using eq. 56 does not differ practically at all from the one we previously found.
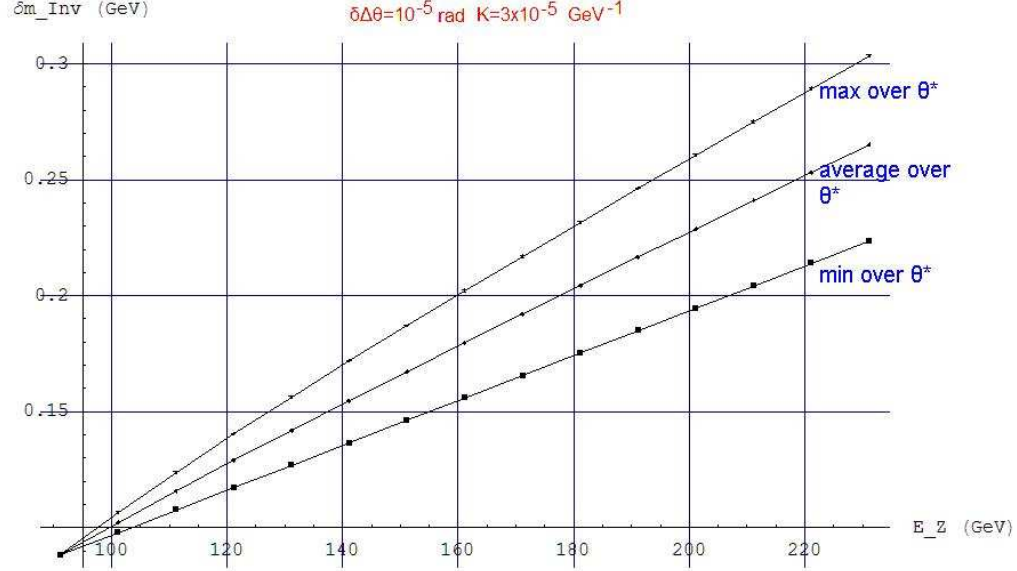
61

Figure 46: The same as fig. 43, but using the Tracker for the determination of the letpons' energy. Tracker gives us an order of magnitude smaller δm_{Inv} than the ECal alone.

To be exact, I should add something more here. Imagine that we have a very high energy ionizing particle. Then, for very big p, eq. 56 would tend to zero. Of course, it does not mean that we would know its angle exactly. It only means that because of its high momentum it did was not deflected much. However, an uncertainty in angles still remains because of the finite granularity of the tracker. As we justified in Appendix B, this granularity-oriented uncertainty is of the order of $G \equiv 10^{-5}\, rad$, so this uncertainty should be *added* to the uncertainty that is coming from the multiple scattering. Then,

$$
\begin{aligned}
\delta\Delta\theta &= \sqrt{(G+D\theta_1)^2 + (G+D\theta_1)^2} \\
&= \sqrt{2G^2 + 2G(D\theta_1 + D\theta_2) + (D\theta_1)^2 + (D\theta_2)^2}
\end{aligned}
\tag{57}
$$

We just saw that G, which is the uncertainty due to granularity, is $G \simeq \sqrt{(D\theta_1)^2 + (D\theta_2)^2}$. Using this,

$$
\delta\Delta\theta \simeq \sqrt{3G^2 + 2G(D\theta_1 + D\theta_2)}
$$

Furthermore,

$$
(D\theta_1 + D\theta_2)^2 = G^2 + 2D\theta_1 D\theta_2 \Rightarrow D\theta_1 + D\theta_2 = \sqrt{2D\theta_1 D\theta_2 + G^2}
$$

so,

$$
\delta\Delta\theta \simeq \sqrt{3G^2 + 2G\sqrt{2D\theta_1 D\theta_2 + G^2}}
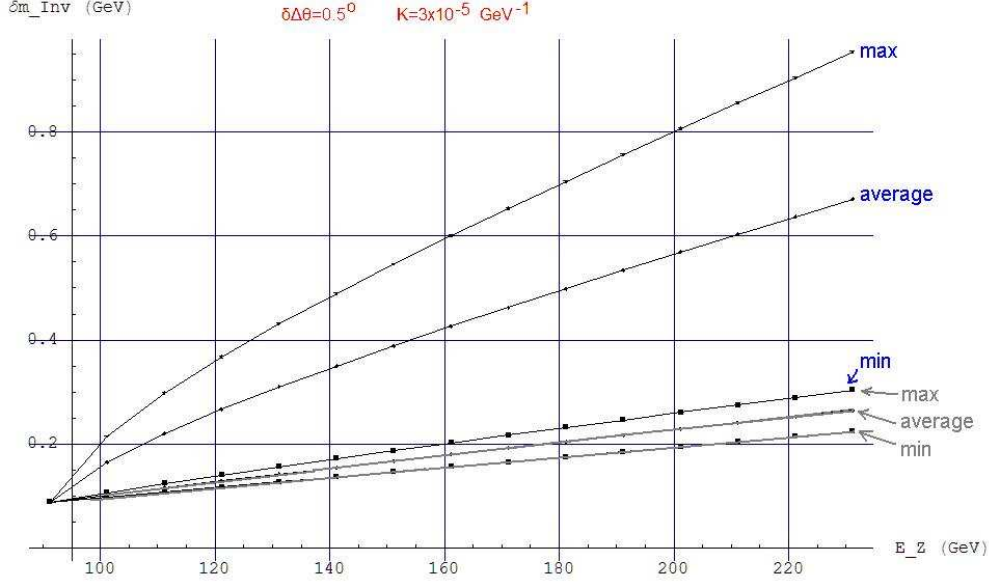$$

62

Figure 47: The same as fig. 44, but using the Tracker for the determination of the letpons' energy. We see how much stronger the dependence on $\delta\Delta\theta$ is when we use the Tracker.

$$
= G\sqrt{3 + 2\sqrt{1 + 2\dfrac{D\theta_1 D\theta_2}{G^2}}}
$$

$$
= G\sqrt{3 + 2\sqrt{1 + 2\dfrac{15 \times 10^{-3}\sqrt{\ell}\frac{1}{p_{e1}} \times 15 \times 10^{-3}\sqrt{\ell}\frac{1}{p_{e2}}}{G^2}}}
$$

$$
= G\sqrt{3 + 2\sqrt{1 + 2\dfrac{1.35 \times 10^{-5}\frac{1}{p_{e1}p_{e2}}}{G^2}}}
$$

I calculated the term $\frac{1}{p_{e1}p_{e2}}$ and I realized that, for $E_Z \in [m_Z,\, 250\,GeV]$, it ranges from 10^{-4} to $5 \times 10^{-4}\,GeV^{-2}$. Taking the second value which is begger (to check the "worst" case), we find

$$
\delta\Delta\theta \;\simeq\; G\sqrt{3 + 2\sqrt{1 + \dfrac{1.35 \times 10^{-8}}{G^2}}}
$$

Putting the value $G = 10^{-5}\,rad$, we get:

$$
\delta\Delta\theta \sim 5.13 \times 10^{-5}\,rad \tag{58}
$$

which is of the same order as G. It was expected of course, since we combined two errors of the same order of magnitude.
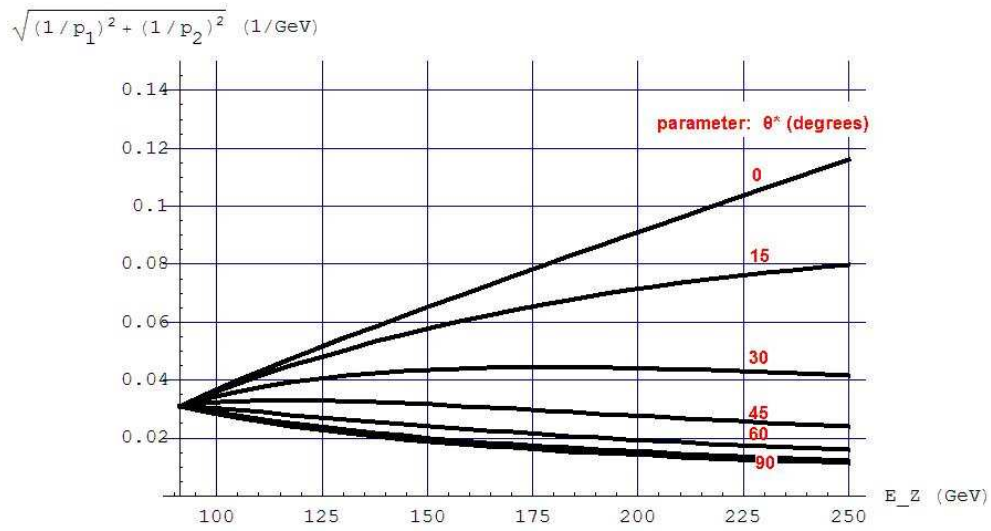
63

Figure 48: The $\sqrt{p_{e1}^{-2} + p_{e2}^{-2}}$ factor for the e^+e^- of a decaying Z.

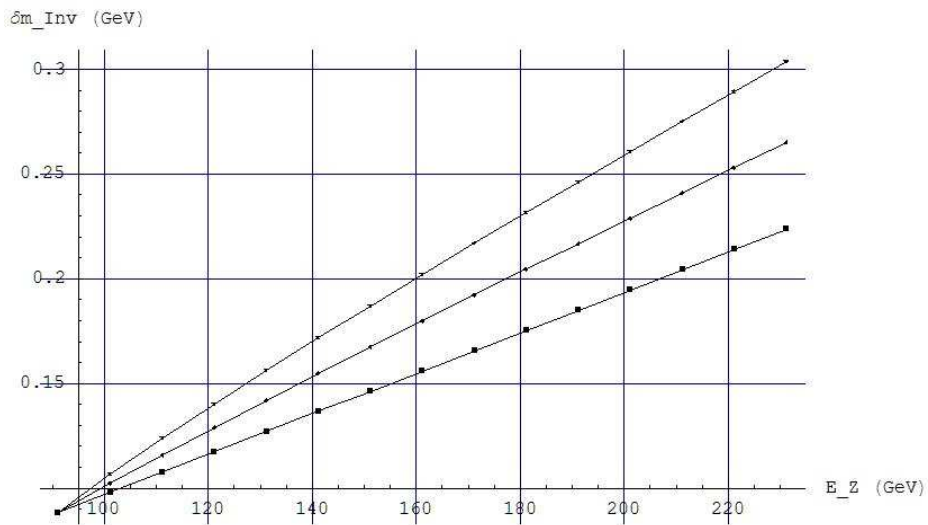Figure 49: The same as fig. 46, but using eq. 57 with $G = 10^{-5}\,rad$ for $\delta\Delta\theta$, instead of assigning a fixed value to it.
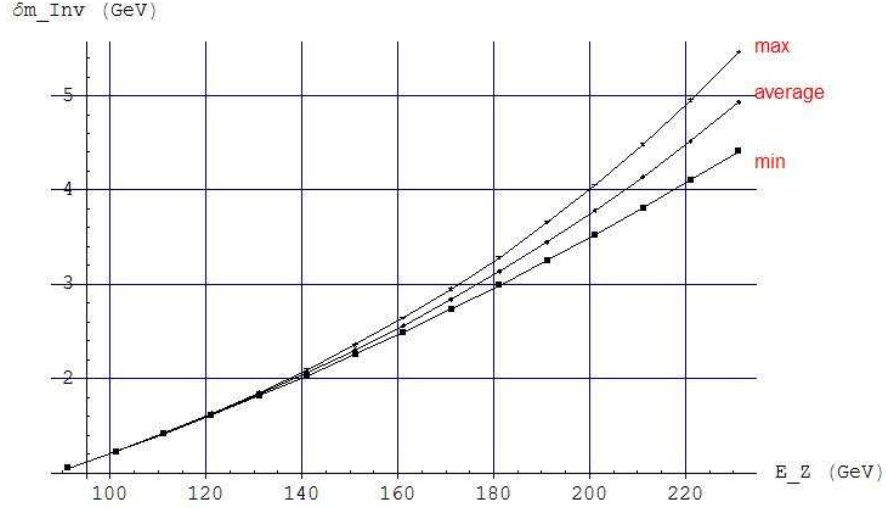
Figure 50: The same as fig. 43, but using eq. 57 with $G = 10^{-5}\,rad$ for $\delta\Delta\theta$, instead of assigning a fixed value to it.

D.4 Combining the Tracker and the ECal

We saw that using only the Tracker gives much smaller δm_{Inv} than using only the ECal.

However, to achieve the best possible accuracy we must use all the information we have, so we must combine the two measurements of the invariant mass.

The formula for the combined error of N independent measurements of the same quantity x with errors δx_1, δx_i ... δx_N is:

$$\delta x = \sqrt{\frac{1}{\sum_{i=1}^{N} \left(\frac{1}{\delta x_i}\right)^2}} \qquad (59)$$

Always, $\delta x \leq \delta x_i \forall i$, and this is the benefit of combining independent measurements. In our case, because the Tracker already is much more accurate than the ECal method, the improvement we achieve by combining the two measurements is very slightly better than the one we already had with the Tracker only. The benefit we have from combining the two errors can be visualized by plotting the difference between $\delta m_{Inv}^{\text{Tracker}}$ and $\delta m_{Inv}^{\text{Combined}}$ (see fig. 51). We see that it is not any bigger than 0.5 MeV, but still, there is no reason not to make the calculation more accurate. The maximum, minimum and average $\delta m_{Inv}^{\text{combined}}$, as functions of E_Z, give a plot whose difference from fig. 49 is invisible.

With such a good invariant mass resolution we can be sure that if a pair of particles is originating from a Z decay we will recognize it as such. The natural width of the Z is about 2.5 GeV and our measurement has at worst an error of about 0.3 GeV (see fig. 49).
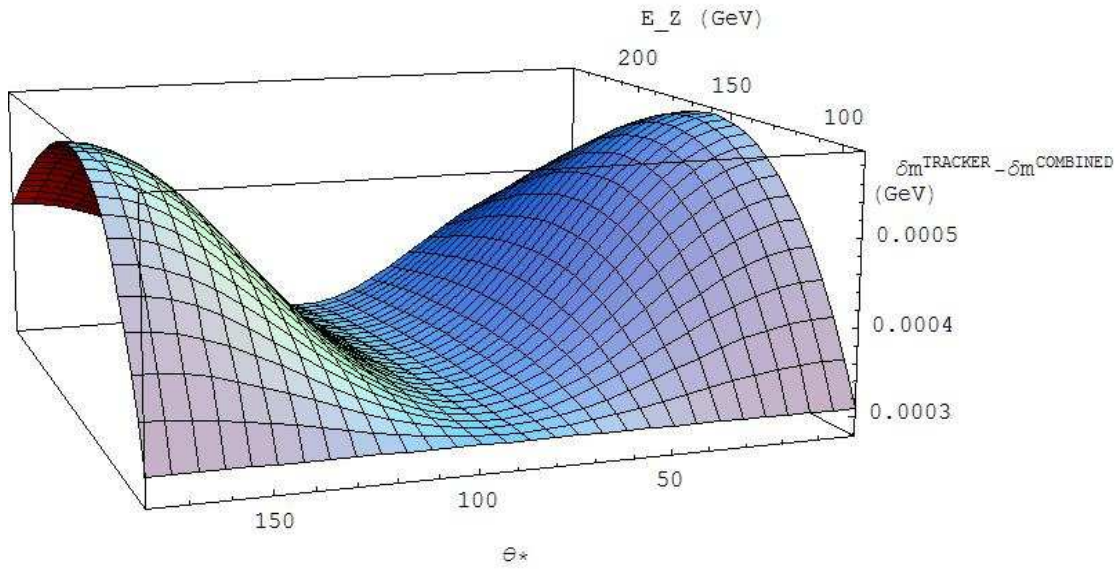
65

Figure 51: As a function of E_Z and θ^*, the difference we gain from the Tracker's error: $\delta m_{Inv}^{Tracker} - \delta m_{Inv}^{\text{combined}}$, assuming multiple scattering with a constant $G = 10^{-5}\,rad$ and $K = 3 \times 10^{-5}\,GeV^{-1}$.